Phytoplankton community structure in contrasting ecosystems of the Southern Ocean: South Georgia, South Orkneys and Western Antarctic Peninsula

Sdena Nunes[a], Mikel Latasa[b] , Maximino Delgado[a], Mikhail Emelianov[a], Rafel Simó[a], Marta Estrada[a]

[a] Institut de Ciències del Mar, CSIC, Pg. Marítim de la Barceloneta, 37-49, 08003 Barcelona, Catalunya, Spain

[b] Centro Oceanográfico de Gijón/Xixón (IEO), Avda. Príncipe de Asturias 70bis, 33212 Gijón/Xixón, Asturias, Spain

e-mail addresses:

Sdena Nunes, sdena@icm.csic.es

Mikel Latasa, mikel.latasa@ieo.es

Maximino Delgado, mdelgadom9@hotmail.com

Mikhail Emelianov, mikhail@icm.csic.es

Rafel Simó, rsimo@icm.csic.es

Marta Estrada, marta@icm.csic.es

Corresponding authors: Sdena Nunes, sdena@icm.csic.es; Marta Estrada, marta@icm.csic.es

Short title: Phytoplankton in contrasting ecosystems of the Southern Ocean

Declarations of interest: none.

ABSTRACT

The relationships between taxonomy and distribution of the phytoplankton and environmental parameters were studied in four contrasting zones (North of the South Orkney Islands= NSO, Southeast of the South Orkney Islands = SSO, Northwest of South Georgia = NSG and West of Anvers = WA) of the Atlantic sector of the Southern Ocean, during the PEGASO cruise of the BIO Hespérides (January-February 2015). The structure of the phytoplankton community was determined by microscopic examination and by pigment analyses using high-performance liquid chromatography (HPLC) followed by application of the CHEMTAX algorithm,. Overall, a statistically significant association was found between fluorometric and HPLC determinations of chlorophyll *a*, and between chemotaxonomic and microscopy-derived estimates of the contribution of diatoms, dinoflagellates and cryptophytes, although the latter appeared to be underestimated by the microscopic observations. The highest average levels of fluorometric chlorophyll *a* (517 mg m^{-2}) were found at NSG, followed by WA (132 mg m^{-2}), NSO (120 mg m^{-2}) and SSO (34 mg m^{-2}). The phytoplankton community at NSG was dominated by diatoms like *Eucampia antarctica* and *Thalassiosira* spp. Cryptophytes and diatoms (mainly *Corethron pennatum*, small *Thalassiosira* spp. and *Fragilariopsis* spp.) were the most abundant chemotaxonomic groups at NSO, followed by haptophytes types 6 + 7, *Phaeocystis*-like (haptophytes type 8) and, especially in the deeper levels of the euphotic zone, pelagophytes. At SSO, the most important groups were haptophytes types 6 + 7, followed by diatoms (with a combination of taxa similar to that of NSO), *Phaeocystis*-like and pelagophytes. The main CHEMTAX groups at WA were cryptophytes (between surface and about 40 m depth), haptophytes types 6 + 7 and diatoms. The ratio between the photoprotective pigment diadinoxanthin and the sum of the light harvesting pigments of diadinoxanthin-containing phytoplankton

sharing (sum of 19'-butanoyloxyfucoxanthin, 19'-hexanoyloxyfucoxanthin, fucoxanthin and peridinin) was highest at SSO, indicating exposure to a high irradiance environment, and presented a significant positive correlation with the euphotic zone depth. The ratios of the algal osmolyte dimethylsulfoniopropionate and the trace gas dimethylsulfide to chlorophyll *a* showed the same pattern across zones, highlighting the role of light-related ecophysiology in combination with taxonomy in regulating the production of dimethylated sulfur by plankton communities.

KEYWORDS: Southern Ocean; phytoplankton distribution; microscopy; HPLC; CHEMTAX; pigments; dimethylated sulfur

1. Introduction

The Southern Ocean (SO) plays a substantial role in regulating and controlling the climate in the world. One of its main features is the Antarctic Circumpolar Current (ACC), which flows clockwise around Antarctica, connecting the Atlantic, Indian and Pacific oceans. The SO covers about 30% of the global ocean and large parts of it are high-nutrient low-chlorophyll (HNLC) areas, mainly due to the co-limitation of light and micronutrients such as iron. Despite widespread limitation to productivity, it is a large sink for anthropogenic CO_2 in the world and accounts for about 43% of the ocean uptake of anthropogenic CO_2 released to the atmosphere over the historical period (Frölicher et al., 2015). This control occurs mainly through CO_2 solubility in the water and by action of the so-called biological pump – CO_2 capture by phytoplankton photosynthesis in surface waters of localized high-productivity areas, vertical transport of organic matter and carbon sequestration in the deep ocean and the sediment (Boyd and Trull, 2007; Marinov et al., 2008). Besides contributing to ocean carbon sequestration, phytoplankton plays a key role in the metabolism of sulfur compounds and may contribute to the formation of organic aerosols. In particular, some phytoplankton groups, such as haptophytes and dinoflagellates, synthesize substantial quantities of dimethylsulfoniopropionate (DMSP), which by enzymatic action can form dimethylsulfide (DMS). These and other biogenic organic emissions can influence the optical properties of the atmosphere and the Earth radiative budget (Charlson et al., 1987; Simó, 2001).

The SO contains very diverse environments, which influence the function and structure of the corresponding phytoplankton communities. One of the key factors appears to be the availability of iron. Open waters of the ACC are generally iron-limited, while coastal regions influenced by terrestrial sources, such as areas neighboring subantarctic islands or the Antarctic Peninsula, may have adequate iron supply (Martin et al., 1990; Moore et al., 2013). Another major abiotic factor influencing phytoplankton growth in the SO is light availability and its interaction with water column mixing, in turn affected by wind forcing and stabilization associated with ice melt (Vernet et al., 2008; Cassar et al., 2011).

Phytoplankton blooms in the Atlantic sector of the SO tend to be dominated by diatoms or haptophytes like *Phaeocystis* spp. (Estrada and Delgado, 1990; Mendes et al., 2013) but cryptophyte proliferations may also be important, in particular in areas influenced by melting ice (Schloss and Estrada, 1994; Moline et al., 2004). Documenting the composition of the phytoplankton communities is important for understanding food web dynamics, biogeochemical cycling and aerosol production, and for projecting potential responses of the ecosystem to climate change.

The PEGASO oceanographic cruise, on board the RV Hespérides was conducted in the Atlantic sector of the SO as part of the PEGASO project, which investigated the role of planktonic community structure, activity and physiological state, in parallel to measurements of aerosol chemistry and physics. The survey included series of oceanographic stations in four contrasting zones (or sub-regions) of the SO, located in the vicinity of the South Orkneys, the South Georgia and the Anvers Islands. The reasoning for selecting these zones was a combination of differences in hydrographic conditions, nutrient availability (in particular with respect to iron) and relatively slow currents without stable direction. A Lagrangian approach using drifters or icebergs as markers was applied within each zone to locate the stations and a suite of physical, chemical and biological measurements was conducted at each of them. Within this context, the present work deals with the quantitative distribution and taxonomic composition of the phytoplankton communities. Previous phytoplankton work in or near our study zones had been based either on microscopy (Priddle et al., 1986; Atkinson et al., 2001; Ward et al., 2008; Garibotti et al., 2005; Luan et al., 2013) or on High Performance Liquid Chromatography (HPLC) determinations (Moline et al., 1997; Gibberd et al., 2013), whith only few studies combining both approaches (Rodríguez et al., 2002; Garibotti et al, 2003; Mendes et al., 2015). We used HPLC analysis of phytoplankton pigments (Roy et al., 2011), followed by application of the CHEMTAX algorithm (Mackey et al., 1996) to estimate the quantitative contribution of major phytoplankton groups (including pelagophytes, which had not been previously assessed in the region) to total chlorophyll a (Chl *a*) and we combined these results with microscopic observations of nano- and microphytoplankton to refine the identification of

the main nano- and microphytoplankton taxa. The specific aims of this study were to compare the results obtained by means of microscopy and HPLC, to use pigment composition to assess physiological variability at diel scales under contrasting ecological conditions and to document the links between phytoplankton community structure and environmental drivers and properties.

2. Material and methods

2.1. PEGASO study location and sampling

This survey was conducted on board the B.I.O. Hespérides in the austral summer of 2015 (From January, 02 to February, 12). Four zones or sub-regions (Fig. 1) were chosen for a several-day study following a Lagrangian approach: north of the South Orkney Islands (NSO), southeast of the South Orkney Islands (SSO), northwest of South Georgia (NSG) and west of Anvers (WA). The position of the main hydrographic fronts during the cruise (Figs. 2 and S1A) was determined, following the scheme of Orsi et al. (1995), with reference to the continuous records of temperature and salinity (thermosalinograph SBE 21 SeaCAT), current velocity and direction measured with the Shipboard Acoustic Doppler Current Profiler (SADCP) "Ocean Surveyor" at 75 khz, and the synoptic modeling data obtained from the Global Real-Time Ocean Forecast System (Global RTOFS) (Dall'Osto et al., 2017). We also consulted 8-day average satellite images of chlorophyll *a* concentration and sea surface temperature obtained from the Visible and Infrared Scanner (VIRS), NASA. We did not measure micronutrients, but evidence from prior studies places NSG as iron-sufficient and considers open sea areas of the ACC as HNLC regions due to iron limitation (Martin et al., 1990; Nielsdóttir et al., 2012). In three of the zones (NSO, NSG and WA), the studied water bodies were marked by means of WOCE (World Ocean Circulation Experiment) standard drifters provided with Iridium communication system; in SSO, icebergs were used as Lagrangian "markers".

Conductivity-temperature-depth (CTD) data were obtained with a SeaBird 911 Plus multi-parametric probe and underway measurements of temperature and conductivity (salinity) were performed with a thermosalinograph (TSG) SBE21. All SBE sensors were calibrated by Sea-Bird Scientific manufacturer according their protocols (https://www.seabird.com/service-calibration-information). For data quality control, a double set of temperature and conductivity

sensors was installed on the CTD probe, and the differences between temperature and conductivity (salinity) data, obtained by at the same time by each pair of temperature or salinity sensors were analyzed during the raw data conversion. Further data processing was performed with Sea-Bird software, following the recommendations of the manufacturer https://www.seabird.com/software. The quality control of underway TSG measurements was performed by periodical sampling of the water input and further salinity analysis on board by means of a Guildline 8410-A Portasal salinometer (http://www.guildline.com/).

CTD casts using the SBE 911 Plus sonde attached to a rosette of 24 12-L PVC Niskin bottles were carried out at least once a day, around 8:30 solar (local) time. In addition, a 36-hour cycle was sampled in each zone, with CTD casts every 4 hours starting generally at 9:30 and ending at 17:00 (solar times) the day after (see Table S1 for station information). Solar time calculations were performed by means of the NASA Solar Calculator (https://www.esrl.noaa.gov/gmd/grad/solcalc/, accessed on 15 December 2017). Conductivity, temperature, depth, *in vivo* fluorescence (with a WET Labs ECO-AFL/FL fluorometer) and photosynthetically active radiation (PAR, measured with a LI-COR Biospherical PAR Sensor) profiles were recorded down to 400 m. Water samples were taken from the Niskin bottles, at six different depths. Generally, these included "surface" (4 m depth), a "deep" level ranging between 120 m and 150 m, and four additional levels in between (Table S1). Fluorometric Chl *a* (Fl_Chl *a*) determination and phytoplankton pigment analyses were carried out for all six depths. Major nutrients, DMS and DMSP were analyzed for surface samples. Water samples for phytoplankton identification by microscopy were collected from surface and the depth of maximum fluorescence, generally the 1% light depth. Mixed layer depth was estimated in as the first depth for which water density was 0.125 kg m^{-3} higher than at surface (Monterey and Levitus, 1997).

2.2. Nutrient concentration, Fluorometric Chl a *(Fl_Chl* a*) and DMS and DMSP determinations*

Water for nutrient analyses was placed (without previous filtration) in Falcon vials and kept frozen at -20ºC until processing in the land laboratory. Phosphate, nitrate, nitrite and

174 silicate concentrations were determined with a Bran+Luebbe AA3 AutoAnalyzer, following the
175 procedures of Hansen & Koroleff (1999).

176 For Fl_Chl *a* determination, 100 cm^3 of water were filtered through Whatman GF/F
177 fibre filters (25 mm diameter), which were subsequently placed in a freezer at −20 °C. After
178 several hours, the filters were introduced in vials with 90% acetone and left in the dark at 4°C
179 for about 24 hours. The fluorescence of the extracts was measured with a Turner Designs
180 fluorometer according to the procedure described in Yentsch and Menzel (1963). No
181 "phaeophytin" correction was applied.

182 Aqueous (GFF-filtered) concentrations of DMS were determined with a purge and trap
183 gas chromatograph (GC) coupled to a mass spectrometry detector; total (particulate + dissolved,
184 largely particulate) DMSP was determined by alkaline hydrolysis of unfiltered samples, analysis
185 by purge and trap GC with flame photometric detection, subtraction of the endogenous DMS
186 (Dall'Osto et al., 2017).

187 *2.3. Phytoplankton identification*

188 Immediately after collection, 250 cm^3 of seawater were placed in amber glass flasks,
189 preserved with formalin-hexamine solution to a final concentration of 1% formalin and stored in
190 the dark until analysis. For phytoplankton identification 100 cm^3 methacrylate settling chambers
191 were filled with the seawater sample. After 48 hours of sedimentation, the chamber bottom was
192 separated and examined under a XSB-1A inverted microscope (Utermöhl, 1958). The entire
193 base of the chambers was scanned at 125X to quantify the less abundant and larger organisms of
194 the microphytoplankton (> 20 µm), and at least two transects were examined at 312X to
195 enumerate the smaller and more abundant organisms of the nanoplankton (< 20 µm). On
196 occasions of exceptionally high concentrations, 6 fields were counted at 312x. Phytoplankton
197 was identified to the species level, when possible. However, many organisms could not be
198 adequately classified and were pooled in categories such as "small dinoflagellates (< 20 µm)",
199 "unidentified centric diatoms" or "unidentified small coccolithophores (< 10 µm)". The inverse
200 microscope method is not adequate for the small organisms of the picoplankton. Our counts,
201 thus, include nano- and microplankton. For the purpose of comparison with the pigment data,

we classified the organisms into the following groups: dinoflagellates, diatoms, coccolithophores, cryptophytes and other. For brevity, we will refer to these groups as "phytoplankton", although many dinoflagellates are heterotrophs. For biovolume estimation, maximum and minimum length, and maximum and minimum width were recorded for each taxon, using a digital camera and the Scope Photo software after calibration for the employed microscope; average values from these measurements were used to calculate the volume of approximate geometric shapes: ellipsoid for dinoflagellates, coccolithophores and flagellates, cylinder for centric diatoms and prisma for pennate diatoms (a simplified version of the shapes proposed by Hillebrand et al., 1999). Biovolume estimates referred to the main part of the body, so that setae and other appendages were not included. The main references for taxonomical identification were Sournia (1986), Ricard (1987), Chrétiennot-Dinet (1990), Rampi and Bernard (1990), Cros and Fortuño (1992), Tomas (1993, 1995) and UNESCO (1995).

2.4. HPLC pigment analysis

Pigment composition was determined by HPLC (Latasa, 2014). Briefly, 0.65 – 1 L of seawater were filtered onto Whatman GF/F (nominal pore size 0.7 µm; 25 mm diameter) glass fiber filter under dim light. The filters were folded, introduced into cryovials and frozen at -80ºC until analysis on land, at the Centro Oceanográfico de Gijón (IEO, Instituto Español de Oceanografía, Spain). For analysis, the filters were placed in Nalgene tubes with 2.5 cm^3 of 90% acetone in which an internal standard of apo-8'-carotenal (Fluka) had been dissolved. The tubes were chilled in ice, sonicated during 30 seconds and stored for 24 hours at - 20 °C. Afterwards, the samples were vortexed, filtered through Whatman GF/F glass fiber filters to remove filter debris and immediately injected into the HPLC instrument [Agilent series (Waldbronn, Germany) 1200 chromatographic system with a G1311A quaternary pump, a G1367C autosampler with a 100 µL capillary loop, a G1316B column thermostat, and a G1315C diode array detector]. Sample extract/water ratios of 60/40 were used, according to Latasa (2014). Pigments (Table 1) were identified at 474 and 664 nm. The total monovinyl-chlorophyll *a* concentration (T_Chl *a*) was estimated as the sum of monovinyl-chlorophyll *a*,

chlorophyllide *a*, chlorophyll *a* epimer and chlorophyll *a* allomers. No divinyl-chlorophyll *a* was detected.

2.5. Photoprotective pigment index

Variations in irradiance intensity may alter the concentrations and composition of phytoplankton pigments (Higgins et al., 2011). To assess the photoacclimation response of at least the part of the phytoplankton sharing diadinoxanthin as the main light-protecting pigment (which includes diatoms, dinoflagellates, haptophytes and pelagophytes), we calculated the ratio Ddx/(LHC) between the concentration of diadinoxanthin (Ddx) and the sum of the concentrations (LHC) of the main light-harvesting carotenoids: fucoxanthin (Fuco), 19'-butanoyloxyfucoxanthin (19-But), 19'-hexanoyloxyfucoxanthin (19- Hex) and peridinin (Per).

2.6. CHEMTAX

The relative abundance of microalgal groups contributing to total Chl *a* biomass was derived from pigment concentration data using version 1.95 of the CHEMTAX chemical taxonomy software (Mackey et al., 1996). This program uses one or several initial matrices of pigment/T_Chl *a* ratios for the selected phytoplankton groups and performs iterations to optimize the proportion of T_Chl *a* accounted for by these groups. The final result of the CHEMTAX program consists of a new adjusted matrix of pigment quotients and a list of the contribution of each pigmentary class to the concentration of each pigment. The initial pigment ratios used in this work were based on diagnostic pigments and pigment matrices used in studies from the Antarctic region (Rodríguez et al, 2002; Kozlowski et al, 2011). The pigments considered were Per, 19-But, 19-Hex, alloxanthin (Allo), chlorophyll *b* (Chl *b*), chlorophyll *c*2 (Chl *c*2), Fuco, lutein (Lut), prasinoxanthin (Pras), violaxanthin (Viol) and zeaxanthin (Zea). The haptophytes, characterized by the occurrence of 19-Hex, were divided in two groups, according to the important presence of 19-But (type 8, which comprises *Phaeocystis*) or to the negligible content of this pigment (a combination of types 6 and 7, including the coccolithophores and *Chrysochromulina*). The samples of each study sub-region were clustered according to the application of Ward's method to a similarity matrix based on Manhattan distances, using the Statistica v.5.5 software. A total of 13 clusters was identified,

corresponding 3 to NSO and SSO, 5 to NSG and 2 to WA. For each cluster, we followed the procedures of Latasa (2007) and Latasa et al. (2010), i.e. we created 29 randomized copies of the initial ratio matrix and we ran the program for eight successive times. After the eighth run, a single average matrix was made and used again for a final run of each cluster (Table S2). Eight pigmentary classes were quantified: Chlorophytes, cryptophytes, diatoms, dinoflagellates, haptophytes types 6 + 7, prasinophytes, haptophytes type 8 (hereafter "*Phaeocystis*-like") and pelagophytes.

2.7. Statistical analyses

The relationships between the CHEMTAX-derived composition of the phytoplankton community at 4 m depth and abiotic parameters (temperature, salinity, oxygen, turbidity, transmission, nitrate, phosphate and Fl_Chl *a*) measured at the same depth plus the MLD of each station were summarized by means of a canonical correspondence analysis (CCA). CHEMTAX-derived Chl *a* values were subjected to a square root transformation to reduce the influence of biomass differences. The calculations were carried out with software package XLSTAT.

3. Results

3.1. General characterization of the study sub-regions

The surface temperature and salinity records and the position of the main hydrographic fronts during the PEGASO cruise are shown in Figs. 2 and S1A. The NSO and the NSG zones were located within meanders of the Southern Boundary of the ACC (SB) and the Polar Front (PF), respectively. SSO, some 60 nautical miles to the north of the Weddell Front, was next to the marginal ice zone of the Weddell Sea. In January 2015, the characteristic position of the Weddell Front coincided with the perimeter of the >25% ice cover (https://seaice.uni-bremen.de – data not shown). WA was placed on the Southern Boundary and was influenced by relatively colder and less saline coastal waters of Anvers Island.

The vertical profiles of temperature, salinity and fluorescence during the time-series sampling and the averages of the environmental parameters for the different study zones are

presented in Fig. 3 and Table 2, respectively. In NSO and SSO (Fig. 3A, B, D and E; Fig. S1B), the layer of relatively cold Winter Water, centered around 70 m depth, was underlain by a relatively warm and saline Warm Deep Water derived from the Circumpolar Deep Water (CDW) of the ACC (Meredith et al. 2011) and was covered by surface layers, seasonally warmed in NSO and influenced by low salinity ice-melt water in SSO. The mean mixed layer depth (MLD) was 30 m in NSO and 16 m in SSO, where it was located just below the ice-melt surface water layer. NSG (Fig. 3G and H; Fig. S1B) was placed outside the main bloom area, which was closer to the continental shelf according to climatological data (Borrione and Schlitzer, 2013) and recent satellite images (data not shown); on the third day of the series, there was a marked change towards warmer, more saline and chlorophyll-poorer surface waters, presumably linked to movements across PF gradients; the MLD was approximately 50 m. The hydrography of the WA (Fig. 3I and J; Fig. S1B) zone is complex (Dinniman and Klinck, 2004); water masses on the shelf are episodically influenced by intrusions of Circumpolar Deep Water. During our visit, mean MLD was 23 m. Average surface nitrate and phosphate concentrations were fairly similar in all zones (the ranges were 27.6-17.2 µM for nitrate and 1.3-2.1 for phosphate, Table 2). In contrast, silicate concentration was 47-50 µM in all sub-regions except NSG, where it was around 2 µM. All zones presented subsurface fluorescence maxima (Fig. 3C, F, I and L), partly related to decreases in the *in vivo* fluorescence/Chl *a* ratio in the upper surface waters (seen also Fig. S2), as will be commented later. Average DMSP and DMS concentrations ranged respectively from 302.8 (NSO) to 83.3 (NSG) and from 8.2 (NSO) to 2.1 (WA); however, the ratios DMSP/Fl_Chl *a* and DMS/Fl_Chl *a* were highest in SSO (Table 2) and lowest in NSG and WA, respectively.

3.2. Phytoplankton pigments

Mean Fl_Chl a concentrations at surface (Table 2) ranged (mean ± SD) from 0.32 ± 0.06 µg L^{-1} at SSO to 5.05 ± 1.98 µg L^{-1} at NSG, with intermediate values for NSO (1.95 ± 0.17 µg L^{-1}) and WA (4.05 ± 0.48 µg L^{-1}). Integrated Fl_Chl *a* values (0–100 m depth) were 33.6 ± 6.2 mg m^{-2} for SSO, 119.8 ± 11 mg m^{-2} for NSO, 132 ± 22.6 mg m^{-2} for WA and 516.8 ± 149.8 mg m^{-2} for NSG. The vertical distribution of Fl_Chl *a* (Fig. S2) was fairly homogeneous

throughout the mixed layer in NSO and NSG, tended to attain the highest values at surface (4 m depth) in WA and presented weak subsurface maxima below the MLD in SSO. In contrast with *in vivo* fluorescence, Fl_Chl *a* did not present surface minima. The ratio Fluo/Fl_Chl *a* between *in vivo* fluorescence (Fluo) and Fl_Chl *a* for the two upper sampling depths showed appreciable circadian variability, with lower values around noon in all sub-regions, as highlighted by significant 2-degree polynomial regressions (Fig. S3A), while for the deeper samples there were no comparable significant relationships (Fig. S3B).

The basic statistical parameters of the pigments determined by HPLC are shown in Table 1 and their average contribution, dominated by Fuco and Chl *c*2 in NSO and NSG, Fuco and 19- Hex in SSO and Fuco, 19-Hex and Allo in WA, is presented in Fig. S4. There was a good correlation between Fl_Chl *a* and T_Chl *a* as determined by HPLC (Fl_Chl *a* = 1.65 *T_Chl *a* + 0.30, n = 268, r^2 = 0.83, p <0.0001) (Fig. S5), although the slope was significantly higher than 1. The ratio between the sum of phaeophorbides and phaeophytines and T_Chl *a* (Phaeo/T_Chl *a*) was calculated as an index of herbivory (Mendes et al., 2015); average values for the two shallower sampling levels of the stations of each sub-region ranged from 10% at WA to 22% at NSG (Table 2). Phaeo/T_Chl *a* was relatively homogeneous in the upper water layers but increased considerably below 50 m at NSG and WA and in the deeper samples of NSO and SSO (data not shown).

The ratio Ddx/LHC, between the concentration of the photoprotective carotenoid Ddx and the sum of the concentrations of the chromophyte light-harvesting carotenoids 19-But, 19-Hex, Fuco and Per, decreased strongly below 20-40 m depth in all sub-regions and presented the highest values in the upper mixed layer of SSO (Table 2, Fig. S6A and B). The circadian variability of Ddx/LHC in surface waters was fairly small, with slightly higher noon values in SSO and WA (Fig. S6C).

3.3. Phytoplankton assemblages.

A total of 116 taxa, including several microzooplankton groups (such as ciliates and Radiolaria), were identified by optical microscopy in the surface and subsurface phytoplankton

samples of the different stations. For each sub-region, the average abundance and biovolume of the most important taxa (in terms of biovolume) that were present in at least 25% of the samples are presented in Table S3; the biovolume contribution of some selected taxa and major groups is shown in Fig. 4. The temporal variability of the Chl *a* contribution (hereafter, referred to as Chl *a* concentration) of the eight phytoplankton groups determined by CHEMTAX is shown in Figs. 5 and S7 – S10, and the corresponding average Chl *a* concentrations for each depth is shown in Fig.6. Comparisons between the contribution to total Chl *a* of the chemotaxonomic groups and microscopy-estimated biovolumes could be carried out for diatoms, autotrophic (and mixotrophic) dinoflagellates and cryptophytes (Fig. S11). The relationship was significant for all three groups (diatoms, $r^2 = 0.68$; autotrophic dinoflagellates, $r^2 = 0.23$; cryptophytes, $r^2 = 0.68$, $p < 0.0001$; $N = 105$, $p < 0.0001$ for all groups).

The four studied sub-regions presented marked differences in phytoplankton composition. Cryptophytes, which decreased with depth, and diatoms, which showed the opposite pattern, were the most abundant CHEMTAX groups at NSO, followed by haptophytes types 6 + 7, *Phaeocystis*-like and pelagophytes (figs. 5A and C, Fig. 6 and Fig. S7); the most important taxa in the corresponding microscopy samples were the diatoms *Corethron pennatum*, *Thalassiosira* spp. (small) and *Fragilariopsis* spp., heterotrophic *Gyrodinium* spp. and large and small (< 20 µm) unidentified dinoflagellates, cryptophytes and nanoflagellates (Table S3, Figs. 4A and C). Haptophytes types 6 + 7, followed by diatoms and *Phaeocystis*-like, both of which increased their contribution deeper in the water column, were the most important CHEMTAX groups at SSO (Figs. 5B and D, and Fig. 6). This sub-region presented a combination of microscopy taxa similar to that of NSO (Table S3, Figs. 4B and D), but with lower *C. pennatum* and *Thalassiosira* spp. (small), higher *Fragilariopsis* spp. abundances and a smaller contribution of cryptophytes; as at NSO, diatoms were relatively more important at depth (Table S3, Figs. 4, 5B and D, Fig. 6 and Fig. S8). NSG, the zone with highest T_Chl *a* concentration, was dominated by diatoms at all depths, both in terms of CHEMTAX-derived Chl *a* and of phytoplankton abundance and biovolume (Figs. 4, 5 E and G, Fig. 6 and Fig. S9), but the warmer water body encountered after day 27 (Fig. 3G) was associated to a marked change in the

368 phytoplankton composition, with lower concentrations of diatoms and increased contributions
369 of chlorophytes and *Phaeocystis*-like (Fig. S9) . The main microscopy taxa both at surface and
370 subsurface levels (Table S3, Figs. 4E and G) were *Eucampia antarctica*, *Fragilariopsis*
371 *kerguelensis*, *Thalassiosira* spp. small, *Thalassiosira* and *Porosira* spp., *Odontella weissflogii*
372 and *Trichotoxon reinboldii*, but there was also a substantial contribution of nanoflagellates. In
373 turn, coccolithophores were practically only present in this sub-region. The main CHEMTAX
374 groups at WA (Figs. 5F and H, Fig. 6 and Fig. S10) were cryptophytes and haptophytes types 6
375 + 7 at the shallowest layers, and haptophytes, diatoms and prasinophytes at depth (below 22 m),
376 while microscopic observations (Table S3, Figs. 4F and H) revealed cryptophytes and
377 nanoflagellates, heterotrophic *Gyrodinium* spp., unidentified dinoflagellates and, in particular at
378 the subsurface levels, diatoms such as *Eucampia antarctica*, *Fragilariopsis kerguelensis* and
379 *Thalassiosira* spp. small.

380 The relationships between the chemotaxonomic phytoplankton groups and the physico-
381 chemical variables and the differences among the four study zones were highlighted by the
382 CCA, which explained 79.2% of the total variance with the two first axes. The first axis (C1)
383 separated NSG on the negative side, from the other sub-regions. Diatoms, which characterized
384 the NSG samples, were associated with high temperature, turbidity, MLD and Chl *a*, and low
385 silicate, nitrate, phosphate and oxygen concentrations, whereas cryptophytes, which were
386 particularly abundant at NSO and WA, appeared on the positive side of C1. The second CCA
387 axis (C2) was mainly related to the variability of nitrate, oxygen and salinity and distinguished
388 the sample clusters from NSO, SSO and WA. This axis depicted a sequence from haptophytes,
389 associated with SSO on the positive, low salinity part of C2, to prasinophytes, which were
390 particularly important in NSO, on the opposite part. The other groups were distributed within
391 intermediate values of C1 and C2.

392

393 **4. Discussion**

394 *4.1. Microscope- vs pigment-based quantification of phytoplankton taxa*

Microscopic observations and the HPLC analysis of biomarker pigments followed by the CHEMTAX algorithm have been successfully used in many phytoplankton studies, either separately or complementing each other (Rodriguez et al., 2002; Kozlowski et al, 2011; Cassar et al., 2015; Mendes el al, 2012; Mendes et al 2018a). Microscopy may provide more precise taxonomic classification and additional ecological information through the observation of different life-cycle stages (such as the presence of resting cysts, auxospore formation or colonial vs. solitary forms), but is biased towards relatively large forms (> 5 µm) of phytoplankton groups with identifiable morphological characteristics, is time-consuming and needs a high level of expertise. In contrast, HPLC/CHEMTAX techniques can provide a comprehensive account of the main phytoplankton groups present in a sample, including those collected in oligotrophic areas (Roy et al., 2011). In the present work, we combined HPLC/CHEMTAX with microscopy observations of selected samples to obtain a robust and consistent view of the phytoplankton composition in the study zones. Comparisons between the two techniques must be interpreted with caution due to taxonomically and environmentally-related variability in biomarker pigments and Chl *a* content per biovolume, and to problems in biovolume estimates and in the microscopical identification of naked and small-celled groups (Kozlowski et al., 2011; Cassar et al., 2015). In this work, we found significant relationships between microscopy and chemotaxonomy for diatoms, autotrophic dinoflagellates and cryptophytes (Fig. S11). A strong correlation (r^2 = 0.68) was observed for diatoms, although there were some points, all belonging to the same station, for which the biovolume estimate was substantially lower than the CHEMTAX estimate, a discrepancy which could be attributed to sampling variability, errors in microscopy or overestimation by CHEMTAX due to contribution to Fuco from unidentified nanoplankton (Cassar et al., 2015). The correlation (r^2 = 0.23) was lower for autotrophic dinoflagellates, a finding that could be attributed to errors in the classification of auto- or heterotrophic forms and to the presence of peridinin-lacking species (Garibotti et al., 2003). The correlation coefficient (r^2 = 0.68) was relatively high for cryptophytes, but there was a disagreement between the two methods concerning their relative contribution to the phytoplankton community, especially at NSO (global average of 2% for microscopy vs 24% for

CHEMTAX), an inconsistency which is likely to be caused by underestimation of the cryptophytes in the microscopic samples, as noted also by Rodríguez et al. (2002) and Cassar et al. (2015). A coarse check of those biovolume vs. Chl *a* relationships (ignoring intercept values) could be obtained from calculations of a theoretical Chl *a* to biovolume ratios, which could be estimated using a standard C/Chl *a* ratio of 50 and the C to biovolume equations from Table 2 of Davies et al. (2016). For diatom and dinoflagellate cells between 5 and 40 µm of diameter this Chl *a*/biovolume value would span, respectively, from $2.6*10^{-6}$ to $0.8*10^{-7}$ (ng μm^{-3}) and from $7.1*10^{-6}$ to $2.3*10^{-6}$, fairly close to the slopes (Fig. S11) obtained from our field samples for diatoms ($6.4*10^{-7}$) and dinoflagellates ($1.35*10^{-6}$); however, the corresponding Chl *a*/biovolume ratios for cryptophytes ("Others") between 5 and 20 µm of diameter would be $3.3*10^{-6}$ to $3.6 *10^{-6}$, well below the slope calculated for cryptophytes ($1.0*10^{-5}$), adding support to a possible underestimation of the latter by microscopy. The HPLC-CHEMTAX approach used in our study provided a comprehensive analysis of the phytoplankton composition and highlighted the importance of groups like cryptophytes, chlorophytes, haptophytes types 6 + 7, *Phaeocystis*-like, pelagophytes and prasinophytes in the global community (Figs. 5 and 6). Organisms of these groups tend to deteriorate easily in fixed samples and are difficult to identify by microscopy. In particular, cryptophytes were more important at NSO, SSO and WA than suggested by the microscopic observations, probably due to underestimation in the microscopic observations as discussed above, while most forms from the other groups that endured fixation became presumably pooled into nano- or microflagellate categories. The detection, in many samples, of *Phaeocystis*-like pigments by HPLC but not of *Phaeocystis* spp. cells by microscopy could be explained the presence of other haptophyte type 8 taxa or of non-colonial forms of *Phaeocystis* spp., which would have been counted as unidentified flagellates.

4.2. Ecophysiological hints from pigment composition

The mid-day decline of the ratio Fluo/Fl_Chl *a* (Fig. S3A) for the shallow samples is a common finding (Estrada et al., 1996; Mignot et al., 2011) and has been related to non-photochemical fluorescence quenching processes (Falkowski and Kolber, 1995; Sackmann et

al., 2008), which in turn are influenced by factors such as community and pigment composition, and nutrient and light conditions. In our data set, the variability of the Fluo/Fl_Chl *a* ratio was particularly marked for SSO (Fig. S3A). This was the sub-region with lowest beam attenuation coefficients and the highest average $Z_{1\%}$/MLD relationship (Table 2), suggesting a higher potential for fluorescence quenching.

Consistent with the variation of specific fluorescence, the highest values of the ratio Ddx/LHC, indicative of the proportion of the photoprotective pigment Ddx with respect to the sum of the light-harvesting carotenoids 19-But, 19-Hex, Fuco and Per, were found throughout the shallow mixed layer of SSO (Fig. S6); at NSO, NSG and WA, the ratios were lower and started to decrease with depth within the upper part of the mixed layer, suggesting a faster time scale of photoacclimation relative to that of vertical mixing in the mixed layer of these sub-regions. The surface Ddx/LHC ratio (Fig. S6A and B) decreased with increasing MLD (Fig. S6D) and beam attenuation coefficient (data not shown), and was positively associated (r^2 = 0.78, N = 35, $p < 0.0001$) with $Z_{1\%}$ (Fig. 8A) in agreement with the expected enhancement of photoprotective pigment concentration with increased exposure to a relatively high irradiance environment (Goericke and Montoya, 1997; Cheah et al., 2017; Russo et al., 2018). Interestingly, the Chl *a*-normalized concentration of DMSP (DMSP/Fl_Chl *a*) exhibited the same pattern across zones as Ddx/LHC, i.e., it increased proportionally with light penetration as depicted by $Z_{1\%}$ (r^2=0.70, N = 34, $p < 0.0001$; Fig. 8B). DMSP is a cellular osmolyte mainly produced and harbored by phytoplankton, where it occurs at intracellular concentrations of up to hundreds of mM. Diatoms and cyanophytes typically are low DMSP producers, with DMSP/Chl *a* ratios between 0 and 4 nmol/µg, whereas haptophytes, dinoflagellates and chrysophytes are strong producers, with DMSP/Chl *a* ratios between 50 and >100 nmol/µg (Stefels et al., 2007). Among other functions, DMSP is suggested to help microalgae cope with oxidative stress by producing reactive oxygen species scavengers (Sunda et al., 2002). Therefore, a combination of taxonomic composition and ecophysiological factors linked to environmental conditions appeared to underlie the distribution of phytoplankton DMSP content across the four sub-regions. While DMSP concentration did not correlate with any phytoplankton group,

DMSP/Fl_Chl *a* was highest at SSO (Table 2), Coinciding with a high proportion of haptophytes (CHEMTAX groups haptophytes types 6 + 7 and *Phaeocystis*-like) in the vicinity of sea ice (Stefels et al., 2018), the elevated exposure to solar radiation as depicted by the high values of the Ddx/LHC ratio, and presumably, also, iron limitation (Stefels et al., 2007). The lowest DMSP/Fl_Chl a ratio in NSG can be explained by the dominance of diatoms and a deeper, hence less illuminated, mixing layer (Bell et al., 2010; Galí and Simó, 2015).

4.3. Phytoplankton assemblages and environmental factors

The four zones visited in this study encompassed a wide spectrum of ecological characteristics. NSG was placed between the Polar Front and the Southern ACC Front (SACCF), in a region characterized by the regular occurrence of spring and summer phytoplankton blooms, fueled by the high concentrations of major nutrients and the availability of iron contributed by the ACC after its passage over the shelf waters around South Georgia (Korb et al., 2004; Whitehouse et al., 2008; Nielsdóttir et al., 2012). The relatively high temperatures in this region (mean ± SD, 4.73ºC ± 0.44) in comparison with other SO areas may also contribute to enhanced phytoplankton proliferation (Korb et al., 2004). The PEGASO stations were outside the main bloom area as seem from satellite imagery (Borrione and Schlitzer, 2013), but presented high Chl *a* concentrations (Tables 1 and 2, Figs. 3I and S2). Moderately lower nitrate and phosphate and much lower silicate concentrations at NSG than in the zones around the South Orkney Islands were consistent with a phytoplankton community dominated by well-silicified diatoms like *Eucampia antarctica*, *Thalassiosira* and *Porosira* spp. and *Odontella weissflogii*, typical of blooms in the area (Atkinson et al., 2001), complemented by substantial populations of haptophytes, including coccolithophores, and pelagophytes, as shown by our microscopy and HPLC-CHEMTAX analyses. However, at the time of our visit, the deep mixing layer of about 50 m compared with an average euphotic depth of 26 m (Table 2), and the relatively low silicate concentrations (average of 2 ± 0.4 µM at surface, Table 2) at the threshold for diatom dominance (Egge and Aksnes, 1992; Atkinson et al., 2001) were probably restricting phytoplankton growth.

The other three sub-regions visited in this study, with lower T_Chl *a* concentrations than NSG, presented macronutrient-replete conditions (Tables 1, 2). Surface silicate concentrations exceeding 47 µM (Table 2), reflected a relatively low diatom contribution (Figs. 4 and 6). Lack of macronutrient depletion is typical of iron-limited regions of the SO (Venables et al., 2010). However, marine areas in the vicinity of islands and the West Antarctic Peninsula region may benefit from some benthic supply of iron from continental shelves (Nielsdóttir et al., 2012), a situation that can explain the relatively high Chl *a* concentrations in NSO and WA (Nielsdóttir et al., 2012; Murphy et al., 2013).

The main nano- and microplankton forms recorded by microscopy in NSO and SSO included the diatoms *Corethron pennatum* and *Fragilariopsis* spp., heterotrophic dinoflagellates like *Gyrodinium* spp. and *Protoperidinium* spp., unidentified autotrophic dinoflagellates, nanoflagellates and cryptophytes, all of which have been recorded in the region. Some differences, like the higher proportion of *Fragilariopsis* spp. in SSO could be attributed to the stronger sea ice influence (Cefarelli et al., 2010), which together with the lowest temperatures and Chl *a* concentrations can be taken as indicative of an earlier stage of phytoplankton bloom development in this zone. In transects across the Scotia Sea, from the vicinity of South Georgia to the South Orkney Islands, Korb et al. (2010) noted the abundance of *Corethron pennatum* and *Fragilariopsis* spp. and suggested that iron limitation could account for the high proportion of heterotrophic dinoflagellates, in agreement with our findings at SSO. On the other hand, some microscopy-based surveys in the South Orkney sub-region encountered a dominance of cryptophytes, prasinophytes and other nanoflagellates (Kopczyńska, 1991; Nielsdóttir et al., 2012). At WA, our CHEMTAX results highlighted the dominance of flagellates like cryptophytes and haptophytes 6 + 7, in agreement with the microscopic observations, which showed a high contribution of unidentified flagellates and cryptophytes, while diatoms were scarce. Several studies have shown the association of cryptophyte populations with shallow mixed layers influenced by ice melting (Schloss and Estrada, 1994; Mendes et al., 2018a; 2018b) and a shift from diatoms to cryptophytes has been described as characteristic of the seasonal phytoplankton succession in the West Antarctic Peninsula region (Garibotti et al.,

2003; Moline et al., 2004; Ducklow et al., 2007; Murphy et al., 2013, Mendes et al., 2018b). The gradient of increased T_Chl *a* concentrations and cryptophyte contribution from SSO to NSO and WA was associated with rising temperatures (Fig. S12), suggesting that it could be related, at least in part, to seasonal succession.

The position of the Chemtax groups in the space of the first axes of the CCA (Fig. 7) reflects in part the relationships discussed above, but it must be taken into account that relationships between biological and hydrographical variables may be the expression of the ecological history of a water body, rather than of direct effects. The association of diatoms with low nutrient concentrations reflects the consumption of major nutrients in the NSG sub-region, while the opposite situation of cryptophytes with respect to diatoms highlights their association to contrasting stages of phytoplankton succession. Other relationships in the graph, such as the association of haptophytes with low salinity and of prasinophytes with high salinity can also be interpreted in the context of a combination of ecological, successional and biogeographical factors.

An examination of the vertical distribution of the different phytoplankton categories reveals some consistent trends in the different study zones. Some groups, like haptophytes types 6 + 7 and *Phaeocystis*-like did not show marked vertical gradients within the euphotic zone. Cryptophytes, as noted above, tended to be more important in surface layers, while diatoms and pelagophytes increased their contribution at subsurface levels (Fig. 6). The ability of diatoms to thrive in relatively low light environments has been noted by a number of authors and has been attributed to features such as increased efficiency of ATP production (Fisher and Halsey, 2016). The increased abundance of pelagophytes in subsurface layers agrees with the observations of Latasa et al. (2017), who noted their preference for deeper levels within the deep chlorophyll maximum.

The average concentration of the biogenic trace gas DMS ranged 2-8 nM across sub-regions, being highest at NSO and SSO and lowest at WA (Table 2). DMS is produced from DMSP through the action of DMSP-lyases from phytoplankton and bacteria. The yield of the DMSP-to-DMS conversion is influenced by phytoplankton taxonomy and irradiance conditions,

but also by ecological factors such as grazing-mediated mortality (Simó et al., 2018) or bacterial community composition and metabolism (Simó et al., 2004; Curson et al., 2011). The ratios DMS/DMSP and DMS/Fl_Chl *a* were highest in SSO, despite the sea-ice marginal bloom was at the early phase of development, with expected low mortality rates. The likely explanation would be the coincidence of high irradiances with a large proportion of haptophytes, including *Phaeocystis*-like cells, which harbor high DMSP-lyase activity (Stefels et al., 2018). The lowest DMS/DMSP and DMS/Fl_Chl *a* ratios in WA are rather surprising, taking into account that the bloom there appeared to be in an advanced stage of development, as depicted by the abundance of protest grazers (data not shown); one reason might be the dominance of cryptophytes, which are poor DMS producers and have not been reported to harbor DMSP-lyases (Stefels et al., 2007).

4.4. Conclusion

As part of the PEGASO project, the main aims of this work were to characterize the ecophysiological variability of the phytoplankton in our study region and to ascertain the links between environmental properties and phytoplankton community structure. Microscopic observations and chemotaxonomic pigment analyses were used to ascertain the quantitative and qualitative composition of the phytoplankton in four contrasting sub-regions in the vicinity of South Georgia (NSG), the South Orkneys (NSO and SSO) and Anvers Islands (WA). Our findings confirmed previous observations such as the dominance of diatoms in the iron-rich South Georgia bloom sub-region, the overall importance of haptophytes and the association of cryptophytes with well-illuminated stratified surface waters influenced by ice melting, but also highlighted the substantial contribution of less well-studied forms such as the pelagophytes, important components of the picoplankton. The light stress condition of the phytoplankton community, an ecophysiological factor that is an important modulator of DMSP and DMS metabolism (Bell et al., 2010) was investigated by means of a photoprotective pigment index, which showed the highest values at SSO, the sub-region with the shallowest mixed layer and the deepest euphotic zone, and the lowest at NSG, where the mixed layer was deepest. The combination of light-adaptation, nutrient and taxonomy patterns regulated specific DMSP and

DMS concentrations, with highly irradiated waters with high proportions of haptophytes being the most geared towards DMSP and DMS production.

5. References

Atkinson, A., Whitehouse, M. J., Priddle, J., Cripps, G. C., Ward, P. and Brandon, M. A., 2001. South Georgia, Antarctica: a productive, cold water, pelagic ecosystem. Mar. Ecol. Prog. Ser. 216, 279–308.

Bell, T. G, Poulton, A. J. and Malin, G., 2010. Strong linkages between dimethylsulphoniopropionate (DMSP) and phytoplankton community physiology in a large subtropical and tropical Atlantic Ocean data set. Glob. Biogeochem. Cycles. 24, GB3009, http://doi:10.1029/2009GB003617.

Borrione, I., Schlitzer, R., 2013. Distribution and recurrence of phytoplankton blooms around South Georgia, Southern Ocean. Biogeosciences. 10, 217-231.

Boyd, P.W., Trull, T.W., 2007. Understanding the export of biogenic particles in oceanic waters: Is there consensus? Prog. Oceanogr. 72, 276–312.

Cassar, N., DiFiore, P.J., Barnett, B.A., Bender, M.L., Bowie, A.R., Tilbrook, B., Petrou, K., Westwood, K.J., Wright, S.W., Lefevre, D., 2011. The influence of iron and light on net community production in the Subantarctic and Polar Frontal Zones, Biogeosciences. 8, 227-237.

Cassar, N., Wright S. W., Thomson P. G., Trull T. W., Westwood K. J., de Salas M., Davidson A., Pearce I., Davies D. M., Matear R. J., 2015. The relation of mixed-layer net community production to phytoplankton community composition in the Southern Ocean. Glob. Biogeochem. Cycles. 29, 446–462. http://doi:10.1002/2014GB004936.

Cefarelli, A.O., Ferrario, M.E., Almandoz, G.O., Atencio, A.G., Akselman, R., Vernet, M., 2010. Diversity of the diatom genus *Fragilariopsis* in the Argentine Sea and Antarctic waters: morphology, distribution and abundance. Polar Biol. 33, 1463.

Charlson, R. J., Lovelock, J. E., Andreae, M. O., Warren, S. G., 1987. Oceanic phytoplankton, atmospheric sulphur, cloud albedo, and climate. Nature. 326, 655–661.

618 Cheah, W., Soppa, M.A., Wiegmann, S., Ossebaar, S., Laglera, L.M., Strass, V.H., Santos-
619 Echeandía, J., Hoppema, M., Wolf-Gladrow, D., Bracher, A., 2017. Importance of deep
620 mixing and silicic acid in regulating phytoplankton biomass and community in the iron-
621 limited Antarctic Polar Front region in summer. Deep-Sea Res. II. 138, 74-85.
622 Chrétiennot-Dinet, M.J. 1990. Atlas du Fitoplancton Marin vol. 3. Éditions du CNRS, Paris,
623 France, 261 pp.
624 Cros, L., and J.M. Fortuño. 2002. Atlas of Northwestern Mediterranean Coccolithophores. Sci.
625 Mar. 66 (Suppl. 1): 7-182.Dall'Osto, M., Ovadnevaite, J., Paglione, M., Beddows, D. C.
626 S., Ceburnis, D., Cree, C., Cortés, P., Zamanillo, M., Nunes, S., Pérez, G.L., Ortega-
627 Retuerta, E., Emelianov, M., Vaqué, D., Marrasé, C., Estrada, M., Sala, M.M., Vidal,
628 M., Fitzsimons, M.F., Beale, R., Airs, R., Rinaldi, M., Decesari, S., Facchini, M.C.,
629 Harrison, R.M., O'Dowd, C., Simó, R., 2017. Antarctic sea ice region as a source of
630 biogenic organic nitrogen in aerosols. Sci. Rep. 7(1), 6047.
631 Curson, R. J., Todd, J. D., Sullivan, M. D., Johnston, A. W. D., 2011. Catabolism of
632 dimethylsulphoniopropionate: Microorganisms, enzymes and genes. Nat. Rev.
633 Microbiol. 9, 849–859.
634 Dall'Osto M., Ovadnevaite J., Paglione M., Beddows D.C.S., Ceburnis D., Cree C., Cortés P.,
635 Zamanillo M., Nunes S.O., Pérez G.L., Ortega-Retuerta E., Emelianov M., Vaqué D.,
636 Marrasé C., Estrada M., Sala M.M., Vidal M., Fitzsimons M.F., Beale R., Airs R.,
637 Rinaldi M., Decesari R., Facchini M.C., Harrison R.M., O'Dowd C., Simó R. 2017.
638 Antarctic sea ice region as a source of biogenic organic nitrogen in aerosols. Scientific
639 Reports, 7: 6047. DOI:10.1038/s41598-017-06188-x.
640 Davies, C.H., Coughlan, A., Hallegraeff, G., Ajani, P., Armbrecht, L., Atkins, N., Bonham, P.,
641 Brett, S., Brinkman, R., Burford, M., Clementson, L., Coad, P., Coman, F., Davies, D.,
642 Dela-Cruz, J., Devlin, M., Edgar, S., Eriksen, R., Furnas, M., Hassler, C., Hill, D.,
643 Holmes, M., Ingleton, T., Jameson, I., Leterme, S.C., Lønborg, C., McLaughlin, J.,
644 McEnnulty, F., McKinnon, A.D., Miller, M., Murray, S., Nayar, S., Patten, R., Pausina,
645 R.A., Pritchard, T., Proctor, R., Purcell-Meyerink, D., Raes, E., Rissik, D., Ruszczyk, J.,

646 Slotwinski, A., Swadling, K.M., Tattersall, K., Thompson, P., Thomson, P., Tonks, M.,
647 Trull, T.W., Uribe-Palomino, J., Waite, A.M., Yauwenas, R., Zammit, A., Richardson,
648 A.J., 2016. A database of marine phytoplankton abundance, biomass and species
649 composition in Australian waters. Scientific Data. 3:160043. http://
650 doi:10.1038/sdata.2016.43. Updated 11 April 2017.

651 Dinniman, M. S., Klinck, J. M., 2004. A model study of circulation and cross-shelf exchange on
652 the west Antarctic Peninsula continental shelf. Deep-Sea Res. II. 51, 2003–2022.

653 Ducklow, H. W., Baker, K., Fraser, W. R., Martinson, D. G., Quetin, L. B., Ross, R. M., Smith,
654 R. C., Stammerjohn, S., Vernet, M., 2007. Marine ecosystems: the West Antarctic
655 Peninsula. Phil. Trans. R. Soc. 362, 67–94

656 Egge, J.K., Aksnes, D.L., 1992. Silicate as a regulating nutrient in phytoplankton competition.
657 Mar. Ecol. Prog. Ser. 83, 281– 289.

658 Estrada, M., Delgado, M., 1990. Summer phytoplankton distributions in the Weddell Sea. Polar
659 Biol. 10, 441-449.

660 Estrada, M., Marrasé, C., Salat, J., 1996. *In vivo* Fluorescence/chlorophyll *a* ratio as an
661 ecological indicator in oceanography. Scientia Marina. 60, 317-325.

662 Falkowski, P.G., Kolber, Z., 1995. Variations in chlorophyll fluorescence yields in
663 phytoplankton in the world oceans. Aust. J. Plant Physiol. 22, 341-355.

664 Fisher, N. L., Halsey K. H., 2016. Mechanisms that increase the growth efficience of diatoms in
665 low light. Photosynth. Res. 129, 183–197.

666 Frölicher, T. L., Sarmiento, J.L., Paynter, D.J., Dunne, J.P., Krasting, J.P., Winton, M., 2015.
667 Dominance of the Southern Ocean in Anthropogenic Carbon and Heat Uptake in
668 CMIP5 Models. J. Climate. 28, 862-886.

669 Galí, M., Simó, R. 2015. A meta-analysis of oceanic DMS and DMSP cycling processes:
670 disentangling the summer paradox. Global Biogeochem. Cycles. 29,
671 doi:10.1002/2014GB004940.

672 Garibotti, I.A., Vernet, M., Kozlowski, W.A., Ferrario, M. E., 2003. Composition and biomass
673 of phytoplankton assemblages in coastal Antarctic waters: a comparison of
674 chemotaxonomic and microscopic analyses. Mar. Ecol. Prog. Ser. 247, 27–42.
675 Garibotti, I.A., Vernet, M., Ferrario, M.E. 2005. Annually recurrent phytoplanktonic
676 assemblages during summer in the seasonal ice zone west of the Antarctic Peninsula
677 (Southern Ocean). Deep-Sea Res. I. 52, 1823-1841.
678 Gibberd, M.J., Kean, E., Barlow, R., Thomalla, S., Lucas, M. 2013. Phytoplankton
679 chemotaxonomy in the Atlantic sector of the Southern Ocean during late summer 2009.
680 Deep-Sea Res. I. 78, 70-78.
681 Goericke, R., Montoya, J.P., 1997. Estimating the contribution of microalgal taxa to chlorophyll
682 *a* in the field-variations of pigment ratios under nutrient- and light-limited growth. Mar.
683 Ecol. Prog. Ser. 169, 98-112.
684 Hansen H.P., Koroleff, F., 1999. Determination of nutrients, in: Grasshoff K, Kremling K,
685 Ehrhardt M (Eds.). Methods of Seawater Analyses. Wiley-VCH, Weinheim, 161–228.
686 Higgins, H.W., Wright, S.W. and Schlüter, L., 2011. Quantitative interpretation of
687 chemotaxonomic pigment data, Phytoplankton Pigments, in: Roy S., Llewellyn C. A.,
688 Egeland E.S., Johnsen G., (Eds.), Characterization, Chemotaxonomy and Applications
689 in Oceanography. Cambridge University Press, Cambridge, 257-313.
690 Kopczyńska E.E., 1991.,Distribution of micro flagellates and diatoms in the sea-ice zone
691 between Elephant Island and the South Orkney Islands (December 1988 — January
692 1989). Pol. Polar Res. 12, 515-528.
693 Korb, R.E., Whitehouse, M.J.,Gordon, M., Ward, P., Poulton, A.J., 2010. Summer
694 microplankton community structure across the Scotia Sea: implications for biological
695 carbon export. Biogeosciences. 7, 343–356. www.biogeosciences.net/7/343/2010/.
696 Kozlowski, W. A., Deutschman, D., Garibotti, I., Trees, C., Vernet, M., 2011. An evaluation of
697 the application of CHEMTAX to Antarctic coastal pigment data. Deep-Sea Res. I. 58,
698 350 –364.

699 Latasa, M., 2007. Improving estimations of phytoplankton class abundances using CHEMTAX.
700 Mar. Ecol. Prog. Ser. 329:13-21.
701 Latasa, M., 2014. A simple method to increase sensitivity for RP-HPLC phytoplankton pigment
702 analysis. Limnol. Oceanogr. Methods. 12, 46–53
703 Latasa, M., Cabello, A.M., Morán, X.A. G., Massana, R., Scharek, R., 2017. Distribution of
704 phytoplankton groups within the deep chlorophyll maximum. Limnol. Oceanogr. 62,
705 665-685.
706 Latasa, M., Scharek, R., Vidal, M., Vila-Reixach, G., Gutiérrez-Rodríguez, A., Emelianov, M.,
707 Gasol, J.M., 2010. Preferences of phytoplankton groups for waters of different trophic
708 status in the northwestern Mediterranean Sea. Mar. ecol. Prog. Ser. 407, 27-42.
709 Luan, Q., Wang, C., Wang, X., Sun, J. Niu, M., Wang, J. 2013. Microphytoplankton
710 communities off the Antarctic Peninsula region in austral summer 2010/2011. Pol. Polar
711 Res. 34, 413–428.
712 Mackey, M.D., Mackey D.J., Higgins H.W., Wright S.W., 1996. CHEMTAX - a program for
713 estimating class abundances from chemical markers: application to HPLC
714 measurements of phytoplankton. Mar. Ecol. Prog. Ser. 144, 265 – 283
715 Marinov, I., Gnanadesikan, A., Sarmiento, J.L.,Toggweiler, J.R., Follows, M., Mignone, B.K.,
716 2008. Impact of oceanic circulation on biological carbon storage in the ocean and
717 atmospheric pCO2. Glob. Biogeochem. Cycles. 22, GB3007.
718 Martin, J, Fitzwater, S., Gordon R., 1990. Iron Deficiency Limits Phytoplankton Growth in
719 Antarctic Waters. Glob. Biogeochem. Cycles. 4, 5–12.
720 Mendes, C.R.B., Kerr, R., Tavano, V.M., Cavalheiro, F.A., Garcia, C.A.E., Dessai, D.R.G.,
721 Anilkumar, N., 2015. Cross-front phytoplankton pigments and chemotaxonomic groups
722 in the Indian sector of the Southern Ocean. Deep-Sea Res. II. 118, 221–232.
723 Mendes, C.R.B., de Souza, M.S., Tavano, V.M., Leal, M.C., Brotas, V., Garcia, C.A.E., 2012.
724 Dynamics of phytoplankton communities during late summer around the tip of the
725 Antarctic Peninsula. Deep-Sea Res. I. 65, 1-14.

726 Mendes, C.R.B., Tavano, V.M., Leal, M.C., Souza, M.S., Brotas, V., Garcia, C.A.E., 2013.
727 Polar Biol. 36, 537–547. http://10.1007/s00300-012-1282-4.
728 Mendes, C.R.B., Tavano, V.M., Kerr, R., Dotto, T.S., Maximiano, T., Secchi, E.R., 2018a.
729 Impact of sea ice on the structure of phytoplankton communities in the northern
730 Antarctic Peninsula. Deep-Sea Res. II. 149, 111-123.
731 http://doi.org/10.1016/j.dsr2.2017.12.003.
732 Mendes, C.R.B., Tavano, V.M., Dotto, T.S., Souza, M.S., Kerr, R., Garcia, C.A.E., Secchi,
733 E.R., 2018b. New insights on the dominance of cryptophytes in Antarctic coastal
734 waters: a case study in Gerlache Strait. Deep-Sea Res. II. 149, 161-170.
735 http://dx.doi.org/10.1016/j.dsr2.2017.02.010.
736 Meredith, M.P., Nicholls, K.W., Renfre, I.A., Boehme, L., Biuw, M., Fedak, M., 2011. Seasonal
737 evolution of the upper-ocean adjacent to the South Orkney Islands, Southern Ocean:
738 Results from a ‘‘lazy biological mooring’’. Deep-Sea Res. II. 58, 1569-1579.
739 Mignot, A., Claustre, H., D'Ortenzio, F., Xing, X., Poteau, A., Ras., J., 2011. From the shape of
740 the vertical profile of in vivo fluorescence to Chlorophyll-a concentration.
741 Biogeosciences. 8, 2391–2406.
742 Moline, M.A., Claustre, H., Frazer, T.K., Schofield, O., Vernet, M., 2004. Alteration of the food
743 web along the Antarctic Peninsula in response to a regional warming trend. Glob.
744 Change Biol. 10, 1973–1980.
745 Moline, M.A., Prézelin, B.B., Schofield, O., 1997. Palmer-LTER: stable inter-annual
746 successional patterns of phytoplankton communities in the coastal waters off Palmer
747 Station, Antarctica. Antarctic Journal, 151–153.
748 Monterey, G. and Levitus, S., 1997. Seasonal Variability of Mixed Layer Depth for the World
749 Ocean. NOAA Atlas NESDIS 14, U.S. Gov. Printing Office, Washimgton D.C. 96 pp.
750 87 figs.
751 Moore, C. M., Mills M. M., Arrigo K. R., Berman-Frank I., Bopp L., Boyd P. Galbraith W., E.
752 D., Geider R. J., Guieu C., Jaccard S. L., Jickells T. D., La Roche J., Lenton T. M.,
753 Mahowald N. M., Marañón E., Marinov I., Moore J. K., Nakatsuka T., Oschlies A.,

754 Saito M. A., Thingstad T. F., Tsuda A., Ulloa O., 2013. Processes and patterns of
755 oceanic nutrient limitation. Nat. Geosci. 6, 701-710.
756 Murphy, E.J.; Hofmann, E.E.; Watkins, J.L.; Johnston, N.M.; Piñones, A.; Ballerini, T.; Hill,
757 S.L.; Trathan, P.N.; Tarling, G.A.; Cavanagh, R.A.; Young, E.F.; Thorpe, S.E.;
758 Fretwell, P., 2013. Comparison of the structure and function of Southern Ocean regional
759 ecosystems: The Antarctic Peninsula and South Georgia. J. Mar. Sys. 109–110, 22–42 .
760 Nielsdóttir, M.C, Bibby, T.S., Moore, C.M., Hinz, D.J., Sanders, R., Whitehouse, M., Korb,
761 R., Achterberg, E.P., 2012. Seasonal and spatial dynamics of iron availability in the
762 Scotia Sea. Mar. Chem. 130–131, 62–72.
763 Orsi, A. H., T. W. Whitworth III, and W. D. Nowlin Jr., 1995. On the meridional extent and
764 fronts of the Antarctic Circumpolar Current. Deep-Sea Res. Part I. 42, 641 – 673.
765 Priddle, J., Heywood, R.B., Theriot, E. 1986. Some Environmental Factors Influencing
766 Phytoplankton in the Southern Ocean Around South Georgia. Polar Biol. 5, 65- 79.
767 Rampi L., Bernard M. 1980. Chiave per la determinazione delle peridinee pelagiche
768 mediterranee. Comitato Nazionale Energia Nucleare- RT/BIO (80)8, Roma, Italy, 193
769 pp.
770 Ricard M. 1987. Diatomophycées. Atlas du Fitoplancton Marin vol.2. Éditions du CNRS. Paris,
771 France, 297 pp.
772 Rodríguez, F., Varela, M., Zapata, M., 2002. Phytoplankton assemblages in the Gerlache and
773 Bransfield Straits (Antarctic Peninsula) determined by light microscopy and
774 CHEMTAX analysis of HPLC pigment data. Deep-Sea Res. II. 49, 723–747.
775 Roy, S., Llewellyn C.A., Egeland E.S., Johnsen G., 2011. Phytoplankton Pigments:
776 Characterization, Chemotaxonomy and Applications in Oceanography. Cambridge
777 University Press, Cambridge.
778 Russo, A.D.P.G., de Souza, M.S., Mendes, C.R.B., Jesus, B., Tavano, V.M., Garcia, C.A.E.,
779 2018. Spatial variability of photophysiology and primary production rates of the
780 phytoplankton communities across the western Antarctic Peninsula in late summer
781 2013. Deep-Sea Res. II. 149, 99–110. https://doi.org/10.1016/j.dsr2.2017.09.021.

Sackmann, B. S., Perry M. J., M. J., Eriksen, C. C., 2008. Seaglider observations of variability in daytime fluorescence quenching of chlorophyll-a in Northeastern Pacific coastal waters. Biogeosci. Discuss. 5, 2839–2865.

Schlitzer, R., 2016. Ocean Data View. http://odv.awi.de.

Schloss, I., Estrada, M., 1994. Phytoplankton composition in the Weddell-Scotia confluence area during austral spring in relation to hydrography. Polar Biol. 14, 77-90.

Simó, R., 2001. Production of atmospheric sulfur by oceanic plankton: Biogeochemical, ecological and evolutionary links, Trends Ecol. Evol. 16, 287–294.

Simó, R., 2004. From cells to globe: Approaching the dynamics of DMS(P) in the ocean at multiple scales, Can. J. Fish. Aquat. Sci. 61, 673–684.

Simó, R., Saló, V., Almeda, R., Movilla, J., Trepat, I., Saiz, E., Calbet, A., 2018. The quantitative role of microzooplankton grazing in dimethylsulfide (DMS) production in the NW Mediterranean. Biogeochemistry 141, 125-142.

Sournia A. 1986. Atlas du Fitoplancton Marin vol.1. Editions du CNRS, Paris, France, 219 p.

Stefels, J., Steinke, M., Turner, S., Malin, G., Belviso, S.. 2007. Environmental constraints on the production and removal of the climatically active gas dimethylsulphide (DMS) and implications for ecosystem modelling. Biogeochemistry 83, 245–275.

Stefels, J., van Leeuwe, M. A., Jones, E. M., Meredith, M. P., Venables, H. J., Webb, A. L., Henley, S. F., 2018 Impact of sea-ice melt on dimethyl sulfide (sulfoniopropionate) inventories in surface waters of Marguerite Bay, West Antarctic Peninsula. Phil. Trans. R. Soc. A 376, 20170169, http://dx.doi.org/10.1098/rsta.2017.0169.

Sunda W., Kieber D.J., Kiene R.P., Huntsman S. 2002. An antioxidant function for DMSP and DMS in marine algae. Nature 418: 317–320.

Tomas, C.R. 1993. Marine Phytoplankton. A Guide to Naked Flagellates and Coccolithophorids. Academic Press, San Diego, USA, 263 pp.

Tomas, C.R. 1995. Identifying Marine Diatoms and Dinoflagellates. Academic Press, San Diego, USA, 598 pp.

UNESCO. 1995. Manual on harmful marine microalgae. In: Hallegraeff G.M., Anderson D.M., Cembella A.D., (eds.) and Enevoldsen H.O. (Tech. Editor). Intergovernmental Oceanographic Commission, Manuals and Guides nº33, Paris, France, 551 pp.

Uthermöhl, H., 1958. Zur Vervolkommung der quantitativen Phytoplankton-methodik. Mitt. Int. Ver. Theor. Angew. Limnol. 9, 1-38

Venables, H., Moore, C. M., 2010. Phytoplankton and light limitation in the Southern Ocean: Learning from high-nutrient, high-chlorophyll areas. J. Geophys. Res. 115, C02015.

Vernet, M., Martinson, D., Iannuzzi, R., Stammerjohn, S., Kozlowski, W., Sines, K., Smith, R., Garibotti, I., 2008. Primary production within the sea-ice zone west of the Antarctic Peninsula: I — Sea ice, summer mixed layer, and irradiance. Deep-Sea Res. II. 5, 2068–2085.

Ward, P., Meredith, M.P., Whitehouse, M.J., Rothery, P. 2008. The summertime plankton community at South Georgia (Southern Ocean): Comparing the historical (1926/1927) and modern (post 1995) records. Prog. Oceanogr. 78, 241–256.

Whitehouse, M.J., Korb, R.E., Atkinson, A., Thorpe, S.E., Gordon, M., 2008. Formation, transport and decay of an intense phytoplankton bloom within the High-Nutrient Low-Chlorophyll belt of the Southern Ocean. J. Mar. Sys. 70, 150–167.

Yentsch, C.S., Menzel D.W., 1963. A method for the determination of phytoplankton chlorophyll and phaeophytin by fluorescence. Deep-sea Res. 10, 221–231

Acknowledgements

The cruise was funded by the Spanish Ministry of Economy and Competitivity through project PEGASO (CTM2012-37615). S. N. was supported with a doctoral fellowship from the National Council of Technological and Scientific Development (CNPq) of Brazil. We thank Martí Galí for providing daily satellite imagery. We are grateful to the captain and crew of the BIO Hespérides, the technicians and researchers that participated in the cruise and the Unidad de Tecnología Marina (UTM) of the CSIC for their valuable help during the cruise. The authors

836 thank Mara Abad for nutrient analyses and Carmen Cabeza for her great help with HPLC
837 sample processing.

838 Table 1. Range (minimum: Min and maximum: Max), mean and standard deviation (SD) of integrated values (in mg m^{-2}) between 0 and 100 m
839 depth of the main phytoplankton pigments and of T_Chl *a* for the study zones. Sub-regions are (See Fig. 1): NSO = North of the South Orkney
840 Islands, SSO = South of the South Orkney Islands, NSG = Northwest of South Georgia Island, WA = West of Anvers Island.

		NSO region				**SSO region**			
Pigment name	**Abbreviation**	**Min**	**Max**	**Mean**	**SD**	**Min**	**Max**	**Mean**	**SD**
19'-butanoyloxyfucoxanthin	19-But	6.96	10.50	8.40	1.15	1.24	4.25	2.27	0.92
19'-hexanoyloxyfucoxanthin	19-Hex	5.82	9.82	7.36	1.39	3.83	8.32	6.11	1.40
α-carotene	α-Car	0.40	0.72	0.52	0.09	0.03	0.16	0.10	0.04
β-carotene	β-Car	0.98	2.08	1.48	0.30	0.27	0.83	0.44	0.16
Alloxanthin	Allo	3.15	6.02	4.76	0.72	0.22	0.50	0.40	0.09
Diadinoxanthin	Ddx	4.59	6.28	5.30	0.54	1.49	3.70	2.68	0.65
Fucoxanthin	Fuco	17.32	24.66	19.70	1.95	2.76	14.74	5.62	3.97
Lutein	Lut	0.24	1.63	0.59	0.38	0.05	0.30	0.13	0.08
Peridinin	Per	0.92	1.97	1.34	0.38	0.30	0.83	0.49	0.17

Prasinoxanthin	Pras	0.18	0.45	0.27	0.07	0.09	0.60	0.34	0.15
Violaxanthin	Viol	0.33	1.74	0.54	0.37	0.05	0.64	0.21	0.18
Zeaxanthin	Zea	0.56	1.23	0.84	0.16	0.20	0.61	0.37	0.11
Chlorophyll *b*	Chl *b*	3.01	4.84	4.08	0.46	0.41	6.96	2.45	1.94
Chlorophyll *c2*	Chl c_2	7.57	15.80	10.77	2.36	1.64	7.22	3.25	1.78
Chlorophyll *c3*	Chl c_3	2.98	7.53	4.84	1.37	1.07	4.91	2.32	1.28
Monovinyl Chlorophyllide *a*	MV-Chlide *a*	0.32	3.40	1.52	1.20	0.55	2.03	1.11	0.49
Monovinyl chlorophyll *a* allomer 1	MV-Chl *a*-allomer1	0.52	1.03	0.77	0.13	0.07	0.37	0.20	0.10
Monovinyl chlorophyll *a* allomer 2	MV-Chl *a*-allomer2	0.30	0.55	0.45	0.07	0.00	0.21	0.09	0.07
Monovinyl chlorophyll *a*	MV-Chl *a*	51.67	77.67	61.33	8.33	10.66	39.96	18.93	9.25
Monovinyl chlorophyll *a* epimer	MV-Chl *a*-epimer	0.78	2.06	1.37	0.44	0.12	0.41	0.21	0.08
∑ pheophorbide *a*	Phaeob	6.36	9.65	7.71	0.92	1.26	3.84	2.66	0.84
∑ phaeophytin *a*	Phaeop	2.27	3.52	2.83	0.42	0.30	1.16	0.79	0.27
Total chlorophyll *a*	T_Chl *a*	56.75	85.5	67	9.21	11.6	43.2	20.8	9.9

841

842

843

Table 1, cont.

Pigment name	Abbreviation	NSG region				WA region			
		Min	Max	Mean	SD	Min	Max	Mean	SD
19'-butanoyloxyfucoxanthin	19-But	4.02	7.49	5.10	0.95	2.07	3.05	2.53	0.37
19'-hexanoyloxyfucoxanthin	19-Hex	9.24	14.65	10.79	1.93	5.92	8.13	6.91	0.86
α-carotene	α-Car	0.13	0.34	0.21	0.07	0.87	2.31	1.53	0.50
β-carotene	β-Car	2.26	7.21	5.11	1.55	0.80	1.37	1.00	0.18
Alloxanthin	Allo	0.47	1.18	0.85	0.25	7.29	19.87	13.48	3.55
Diadinoxanthin	Ddx	10.00	31.24	22.38	6.63	2.93	4.97	3.74	0.66
Fucoxanthin	Fuco	57.14	236	155	54.07	9.12	17.05	12.52	2.35
Lutein	Lut	0.38	0.52	0.46	0.05	0.57	1.24	0.81	0.23
Peridinin	Per	2.88	4.40	3.73	0.47	0.28	0.69	0.43	0.12
Prasinoxanthin	Pras	0.40	0.79	0.60	0.10	0.35	0.55	0.42	0.06
Violaxanthin	Viol	0.13	0.49	0.22	0.10	0.09	0.14	0.11	0.02

Zeaxanthin	Zea	2.44	6.39	4.27	1.18	0.41	0.80	0.60	0.14
Chlorophyll *b*	Chl *b*	1.13	2.32	1.62	0.40	1.02	1.47	1.18	0.13
Chlorophyll *c2*	Chl c_2	25.06	89.54	58.69	17.94	8.08	17.29	11.17	2.94
Chlorophyll *c3*	Chl c_3	11.29	36.09	24.38	6.96	2.80	6.71	4.42	1.32
Monovinyl Chlorophyllide *a*	MV-Chlide *a*	1.04	13.66	3.19	3.53	0.37	0.75	0.48	0.12
Monovinyl chlorophyll *a* allomer 1	MV-Chl *a*-allomer1	1.42	4.61	2.70	1.00	0.45	1.21	0.83	0.29
Monovinyl chlorophyll *a* allomer 2	MV-Chl *a*-allomer2	0.85	2.83	1.92	0.57	0.24	0.45	0.35	0.07
Monovinyl chlorophyll *a*	MV-Chl *a*	123	374	254	73.9	31.73	78.15	52.63	13.78
Monovinyl chlorophyll *a* epimer	MV-Chl *a*-epimer	3.85	7.82	5.64	1.34	0.23	1.08	0.83	0.25
∑ phaeophorbide *a*	Phaeob	35.75	81.22	59.30	11.43	6.60	8.69	7.42	0.65
∑ phaeophytin *a*	Phaeop	9.08	21.87	16.41	4.35	1.34	2.41	1.87	0.35
Total chlorophyll *a*	T_Chl *a*	135	408	282	80.9	37.2	85.9	60	14.5

Table 2. Mean ± standard deviation of physico-chemical variables and ratios for the surface samples (except for Phaeo/T_Chl *a* and Ddx/LHC, which are averages for the two shallower sampling dephts), upper mixed layer depth (MLD), depth receiving 1% of surface irradiance ($Z_{1\%}$) and mean of the ratio between $Z_{1\%}$ and MLD for the stations of the studied regions (see Table 1 for sub-region acronyms). Variable abbreviations are: Fl_Chl *a* = fluorometric Chl *a*, DMSP = total (particulate + dissolved) dimethyl sulfoniopropionate, DMS = aqueous dimethyl sulfide, Phaeo = sum of phaeopigments and phaeophorbides (µg L^{-1}), T_Chl *a* = total Chl *a* (µg L^{-1}) Ddx = diadinoxanthin (µg L^{-1}), LHC = sum of 19-But + 19-Hex + fucoxanthin + peridinin (µg L^{-1}). One outlier of Phaeo/T_Chl *a* for station 45, 13 m has been excluded.

Region		**NSO**		**SSO**		**NSG**		**WA**	
	Units	**Mean**	**SD**	**Mean**	**SD**	**Mean**	**SD**	**Mean**	**SD**
Temperature*	ºC	0.58	0.17	-0.75	0.10	4.73	0.44	1.45	0.08
Salinity*		33.84	0.07	33.16	0.06	33.74	0.02	33.41	0.03
Oxygen*	µM kg^{-1}	320.3	1.004	312.4	0.82	295.6	7.52	309.3	1.87
Turbidity*	NTU**	0.56	0.01	0.49	0.003	0.69	0.06	0.55	0.01
Transmission*	%	84.31	1.09	92.23	0.30	83.45	2.98	77.54	1.84
Nitrate*	µM	27.31	1.90	27.55	3.25	17.17	1.63	18.71	0.89
Nitrite*	µM	0.23	0.06	0.16	0.02	0.29	0.04	0.19	0.03
Ammonium	µM	2.86	3.51	1.62	1.06	1.71	1.90	3.08	1.87
Silicate*	µM	47.89	4.07	47.34	4.65	2.00	0.39	49.68	3.66
Phosphate*	µM	1.99	0.21	2.14	0.25	1.29	0.15	1.79	0.16

Fl_Chl *a**	µg L^{-1}	1.87	0.22	0.32	0.02	5.05	0.60	4.05	0.48
MLD*	m	29.75	11.84	15.79	5.35	49.83	11.42	22.89	5.60
$Z_{1\%}$	m	50.0	8.0	89.6	10.0	26.0	6.7	35.0	3.1
$Z_{1\%}$/MLD		2.2	1.5	5.6	1.6	0.6	0.2	1.5	0.3
DMSP	nM	302.8	51.91	89.67	18.35	83.28	27.31	115.7	14.61
DMS	nM	8.19	1.64	7.88	1.52	5.97	1.11	2.13	0.55
DMS/DMSP		0.03	0.01	0.09	0.03	0.08	0.04	0.02	0.004
DMSP/Fl_Chl *a*	nmol/µg	162.5	35.85	291.6	64.61	18.78	9.71	28.68	3.11
DMS/Fl_Chl *a*	nmol/µg	4.33	0.72	24.40	3.88	1.52	0.72	0.53	0.12

844

845 * Variables used in the canonical correspondence analysis

846 ** Nephelometric Turbidity Unit

847 **Explanations of the figures**

848 Figure 1. Position of the sampling stations in the four visited zones: NSO = North of the
849 South Orkney Islands, SSO = South of the South Orkney Islands, NSG = Northwest of
850 South Georgia Island, WA = West of Anvers Island.

851 Figure 2. Track of the research vessel, with sea surface temperatures (A) and salinity
852 (B), recorded with a flow-through termosalinograph, coded in color. The position of the
853 main oceanic fronts across the track is indicated: Polar Front (PF; 50ºS), Southern
854 Antarctic Circumpolar Current Front (SACCF¸56.8ºS-57.2ºS), Southern Boundary of
855 the Antarctic Circumpolar Current (SB; 59.9ºS), and Weddell Scotia Confluence Zone
856 (WSCZ; 60.0ºS-60.8ºS). Figure produced with the Ocean Data View software
857 (Schlitzer, 2016).

858 Figure 3. Vertical profiles of (A, D, G, J) temperature (ºC), (B, E, H, K) salinity and (C,
859 F, I, L) fluorescence (arbitrary units) during the visits to the NSO (A, B, C), SSO (D, E,
860 F), NSG (G, H, I) and WA (J, K, L) sub-regions. The colors represent the day of the
861 year 2015 (color scale on the right side). See the explanation of Fig. 1 for acronyms.
862 Figures produced with the Ocean Data View software (Schlitzer, 2016).

863 Figure 4. Biovolume of selected taxa and major phytoplankton groups in the surface (4
864 m) and subsurface ("deep") samples taken in the four study regions. The labels of the
865 abscissa in the "deep" samples indicate the cast number followed by the sampling depth
866 in m. Acronyms as in Fig. 1.

867 Figure 5. Contribution (in ng l^{-1}) to total chlorophyll *a* by the CHEMTAX-derived
868 phytoplankton groups in surface (4 m) and subsurface (deep) samples taken in the four
869 study regions. The labels of the abscissa in the "deep" samples indicate the cast number

870 followed by the sampling depth in m (when possible, this depth was chosen to match
871 that of Fig. 4). Acronyms as in Fig. 1.

872 Figure 6. Vertical distribution of the mean contribution to total chlorophyll a by the
873 CHEMTAX-derived phytoplankton groups (in ng l^{-1}) in the four study sub-regions.
874 Acronyms as in Fig. 1.

875 Figure 7. Canonical correspondence analysis ordination plot of chemotaxonomic
876 phytoplankton composition and abiotic parameters at surface (along with MLD). The
877 first two axes explain 79.2% of the variance. Arrows indicate environmental variables
878 [temperature (Temp), salinity (Sal), oxygen (Ox), turbidity (Tur), Transmission (Tr),
879 nitrate (NO3), nitrite (NO2), silicate (SiO4), phosphate (PO4), mixed layer depth
880 (MLD), Fl_Chl *a*]. Phytoplankton groups (diamonds) are chlorophytes (Chloro),
881 cryptophytes (Crypt), diatoms (Diat), dinoflagellates (Dino), haptophytes (Hapto),
882 pelagophytes (Pelag), *Phaeocystis*-like (Phaeo), prasinophytes (Pras). Samples of the
883 four sub-regions (circles) are encircled; See the explanation of Fig. 1 for acronyms.

884 Figure 8. Relationship of the euphotic zone depth ($z_{1\%}$, m) with the ratio Ddx/LHC (A)
885 and the ratio DMSP/Fl_Chl *a* (B) for the study sub-regions. The equations are $y = 0.08$
886 $+ 0.0055x$, $r^2 = 0.78$, $N = 35$, $p < 0.0001$ (A) and $y = -60.35 + 3.88x$, $r^2=0.70$, $N = 34$
887 (one outlier eliminated), $p < 0.0001$ (B). Acronyms as in Fig. 1.

888

889

Supplementary material

Supplementary tables: Explanations

Table S1. Position, date, time and sampled depths of the PEGASO stations considered in this work. Sub-regions are (See Fig. 1): NSO = North of the South Orkney Islands, SSO = South of the South Orkney Islands, NSG = Northwest of South Georgia Island, WA = West of Anvers Island. *Time of 2 February 2015.

Table S2. Pigment ratios used for the runs of the different CHEMTAX clusters. The numbers indicate the amount of pigment per unit of Chl *a*. See Table 1 for pigment name abbreviations.

Table S3. Mean and standard deviation (SD) of (A) the abundance in cells l^{-1} and (B) biovolume in μm^3 cm^{-3} of selected taxa and major phytoplankton groups identified in the microscopic observations for the surface (4 m depth) and subsurface (depths as indicated in Fig. 7) samples of the four studied sub-regions. The chosen taxa were those with total biovolume (for the whole data set) exceeding $3*10^5$ μm^3 cm^{-3} and present in at least 25 % of the samples.

Supplementary material

Supplementary figures: Explanations.

Figure S1. A) Main fronts in the PEGASO cruise area (from Dall'Osto et al., 2017). Fronts of the Antarctic Crcumpolar Current (ACC) are marked (Polar Front, PF; Southern ACC Front, SACCF), as is the southernmost limit of the ACC (Southern Boundary, SB). The Weddell Front (WF), marking the southern limit of the Weddell–Scotia Confluence is also shown. The background plot shows the average position of the fronts as depicted by Orsi et al (1995); the color lines are the positions of the fronts nearest to the PEGASO cruise track in Jan-Feb 2015, as reconstructed from underway measurements, satellite data and synoptic modelling (see Dall'Osto et al., 2017). Dashed lines show the portions of the fronts that were crossed by the ship track. B) T-S diagrams for the study zones: 1 = NSO (North of the South Orkney Islands), 2 = SSO (South of the South Orkney Islands), 3 = NSG (Northwest of South Georgia Island), 4 = WA (West of Anvers Island). The color coding (scale on the right side of the graph) indicates *in vivo* fluorescence (arbitrary units).

Figure S2. Vertical distribution of the concentration of fluorometric chlorophyll *a* (Fl_Chl *a*, ng l^{-1}) in (A), the NSO (North of the South Orkney Islands) and SSO (South of the South Orkney Islands) sub-regions, and (B), the NSG (Northwest of South Georgia Island) and WA (West of Anvers Island) sub-regions.

Figure S3. Variation of the *in vivo* fluorescence/ Fl_Chl *a* ratio (Fluo/Fl_Chl *a*) with solar time in (A) the two upper sampling depths and (B) the deeper sampling depths of the four study regions. NSO = North of the South Orkney Islands, SSO = South of the South Orkney Islands, NSG = Northwest of South Georgia Island, WA = West of Anvers Island. The fitted lines are 2-degree

polinomials with the following equations: (A) NSO, $y = -0.15*x + 0.0067*x^2 + 1.37$, $r^2 = 0.55$, $p < 0.0001$; SSO, $y = -0.48*x + 0.02*x^2 + 3.37$, $r^2 = 0.69$, $p < 0.0001$; NSG, $y = -0.23*x + 0.12*x^2 + 1.73$, $r^2 = 0.49$, $p < 0.01$; WA, $y = -0.063*x + 0.0034*x^2 + 0.85$, $r^2 = 0.45$, $p < 0.05$. The polynomial regressions were not significant for the deep data in B.

Figure S4. Mean concentration ± standard deviation (SD), for ach study sub-region, of the ten pigments used in the CHEMTAX algorithm. NSO = North of the South Orkney Islands, SSO = South of the South Orkney Islands, NSG = Northwest of South Georgia Island, WA = West of Anvers Island.

Figure S5. Relationship between Fl_Chl *a* (Fl_Chl *a*) and HPLC-measured total chlorophyll *a* (T_Chl *a*). The equation of the regression line is Fl_Chl $a = 1.65*$ T_Chl $a + 0.30$ ($n = 268$, $r^2 = 0.83$, $p < 0.0001$).

Figure S6. Variability of the ratio Ddx/LHC between diadinoxanthin (Ddx) concentration and the sum of 19-But, 19-Hex, Fuco and Per (see Table 1 for abbreviations) concentrations. (A) vertical distribution of Ddx/LHC in NSO (North of the South Orkney Islands) and SSO (South of the South Orkney Islands) regions, (B) vertical distribution of Ddx/LHC in NSG (Northwest of South Georgia Island) and WA (West of Anvers Island) regions, (C) variation of the Ddx/LHC ratio with solar time in the two upper sampling depths of the four study regions and (D) relationship of Ddx/LHC with the mixed layer depth (MLD).

Figure S7. Temporal variation of the contribution (in ng l^{-1}) to total chlorophyll *a* by the CHEMTAX-derived phytoplankton groups in the NSO (North of the South Orkney Islands) sub-region. Figure produced using the Ocean Data View software (Schlitzer, 2016).

Figure S8. Temporal variation of the contribution (in ng l^{-1}) to total chlorophyll *a* by the CHEMTAX-derived phytoplankton groups in the SSO (South of the South Orkney Islands) sub-region. Figure produced using the Ocean Data View software (Schlitzer, 2016).

Figure S9. Temporal variation of the contribution (in ng l^{-1}) to total chlorophyll *a* by the CHEMTAX-derived phytoplankton groups in the NSG (Northwest of South Georgia Island) sub-region. Figure produced using the Ocean Data View software (Schlitzer, 2016).

Figure S10. Temporal variation of the contribution (in ng l^{-1}) to total chlorophyll *a* by the CHEMTAX-derived phytoplankton groups in the WA (West of Anvers Island) region. Figure produced using the Ocean Data View software (Schlitzer, 2016).

Figure S11. Relationship between biovolume calculated by microscopy and CHEMTAX-derived contribution to T_Chl *a* for (A) diatoms, (B) autotrophic dinoflagellates and (C) cryptophytes. The lines are standard major axis regression lines and their equations are: y = 6.4e-7 x – 135.8 (r^2 = 0.68) for diatoms, y = 1.3e-6x + 3.8 (r^2 = 0.23) for autotrophic dinoflagellates and y = 9.0e-6 x + 25.9 (r^2 = 0.68) for cryptophytes; (N = 105, $p < 0.0001$ for all groups).

Figure S12. (A) Relationship between temperature and T_Chl *a* for the surface level (4 m depth) of the four study regions; (B) relationship between temperature and percentage contribution of cryptophytes to T_Chl *a* in NSO, SSO and WA (there were practically no cryptophytes at NSG). NSO = North of the South Orkney Islands, SSO = South of the South Orkney Islands, NSG = Northwest of South Georgia Island, WA = West of Anvers Island.

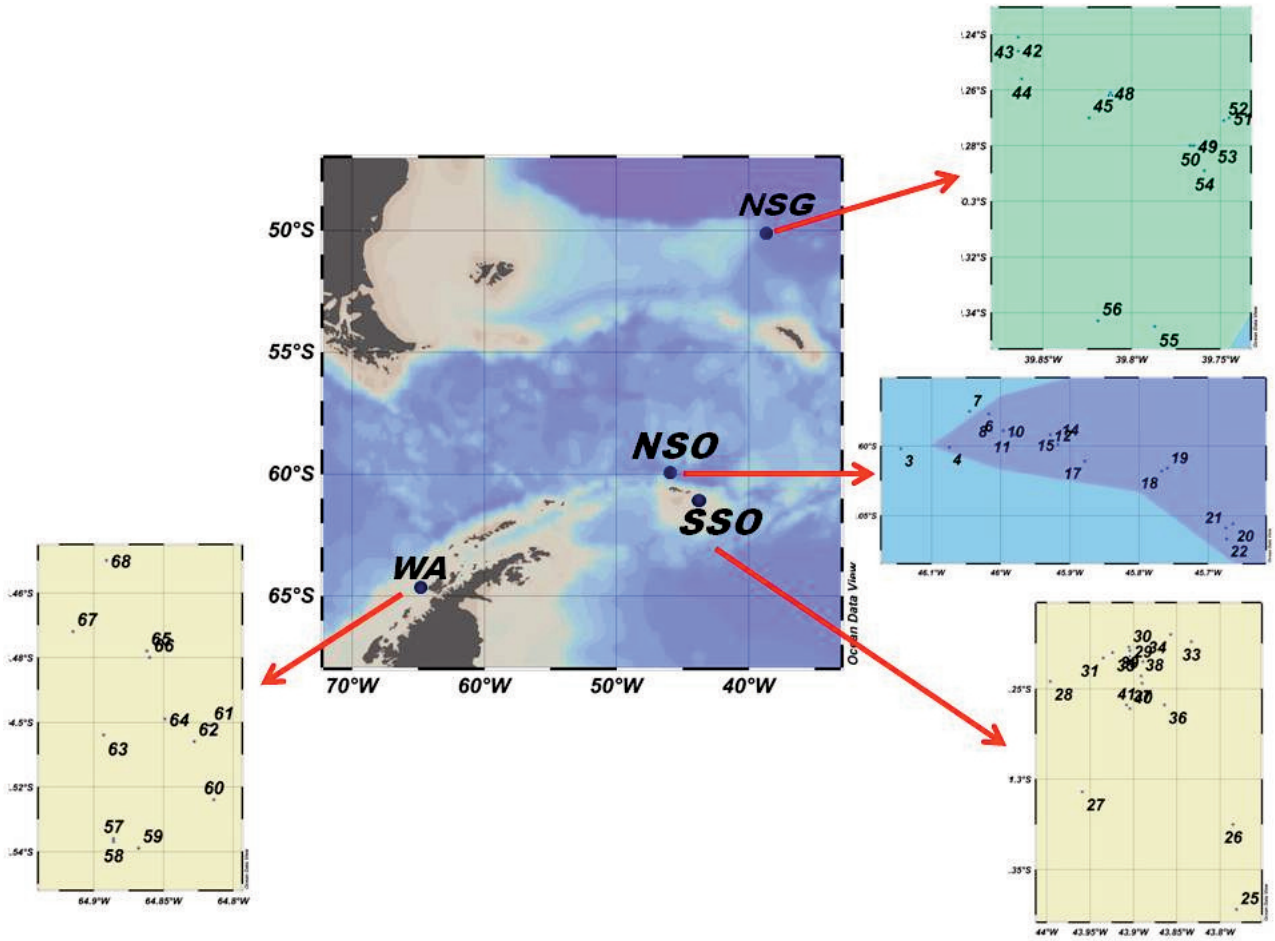

Figure 1

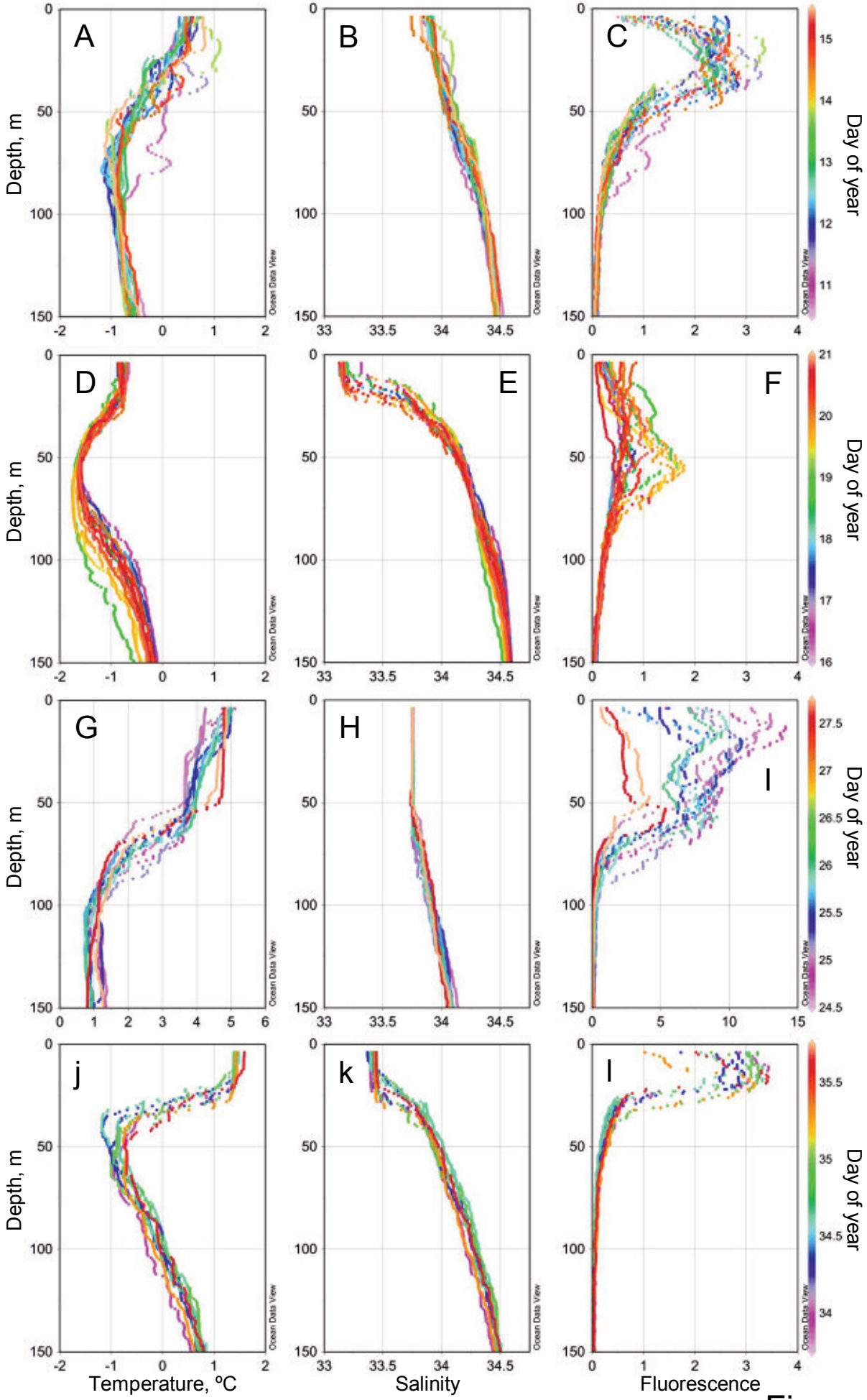
A
B
C
D
E
F
G
H
I
j
k
l
Depth, m
Day of year
Temperature, ºC
Salinity
Fluorescence
Ocean Data View

Figure 3

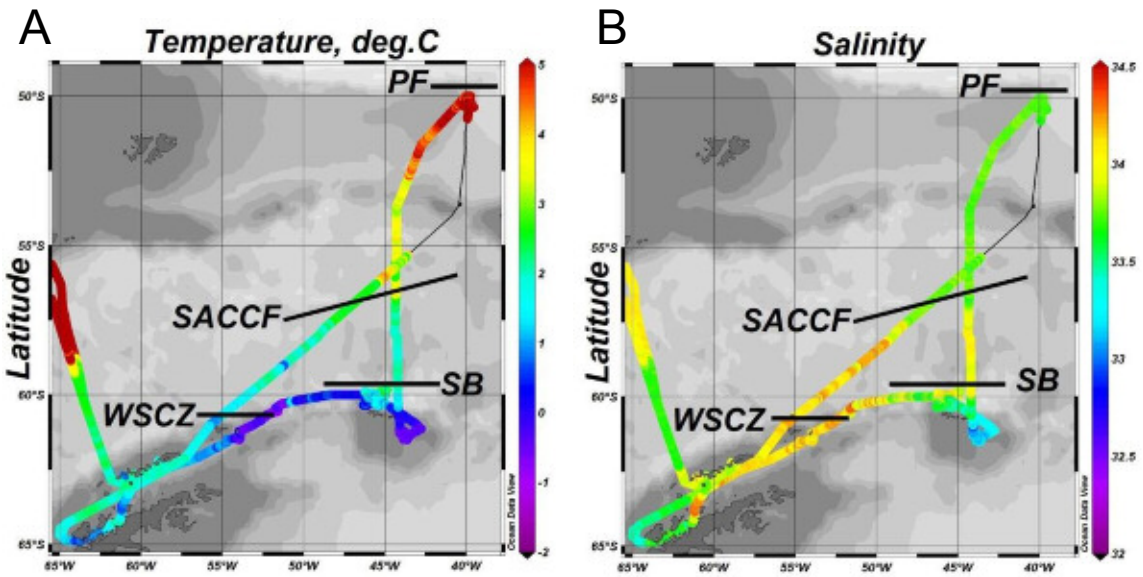
A
Temperature, deg.C
PF
SACCF
SB
WSCZ
Latitude
50°S
55°S
60°S
65°S
65°W
60°W
55°W
50°W
45°W
40°W
5
4
3
2
1
0
-1
-2
Ocean Data View
B
Salinity
PF
SACCF
SB
WSCZ
Latitude
50°S
55°S
60°S
65°S
65°W
60°W
55°W
50°W
45°W
40°W
34.5
34
33.5
33
32.5
32
Ocean Data View

Figure 2

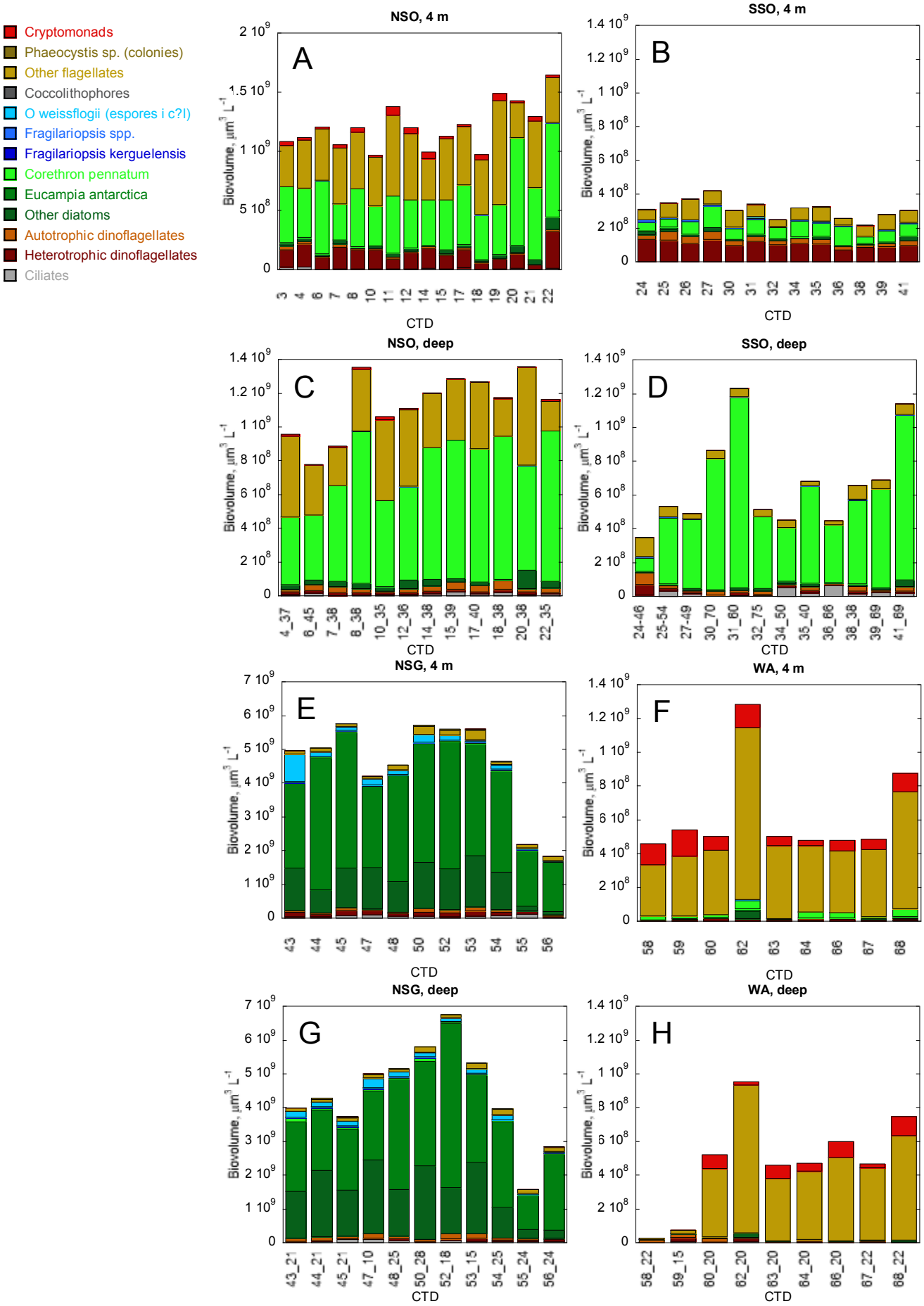
Cryptomonads
Phaeocystis sp. (colonies)
Other flagellates
Coccolithophores
O weissflogii (espores i c?l)
Fragilariopsis spp.
Fragilariopsis kerguelensis
Corethron pennatum
Eucampia antarctica
Other diatoms
Autotrophic dinoflagellates
Heterotrophic dinoflagellates
Ciliates
NSO, 4 m
A
SSO, 4 m
B
NSO, deep
C
SSO, deep
D
NSG, 4 m
E
WA, 4 m
F
NSG, deep
G
WA, deep
H
Biovolume, µm3 L-1
CTD

Figure 4

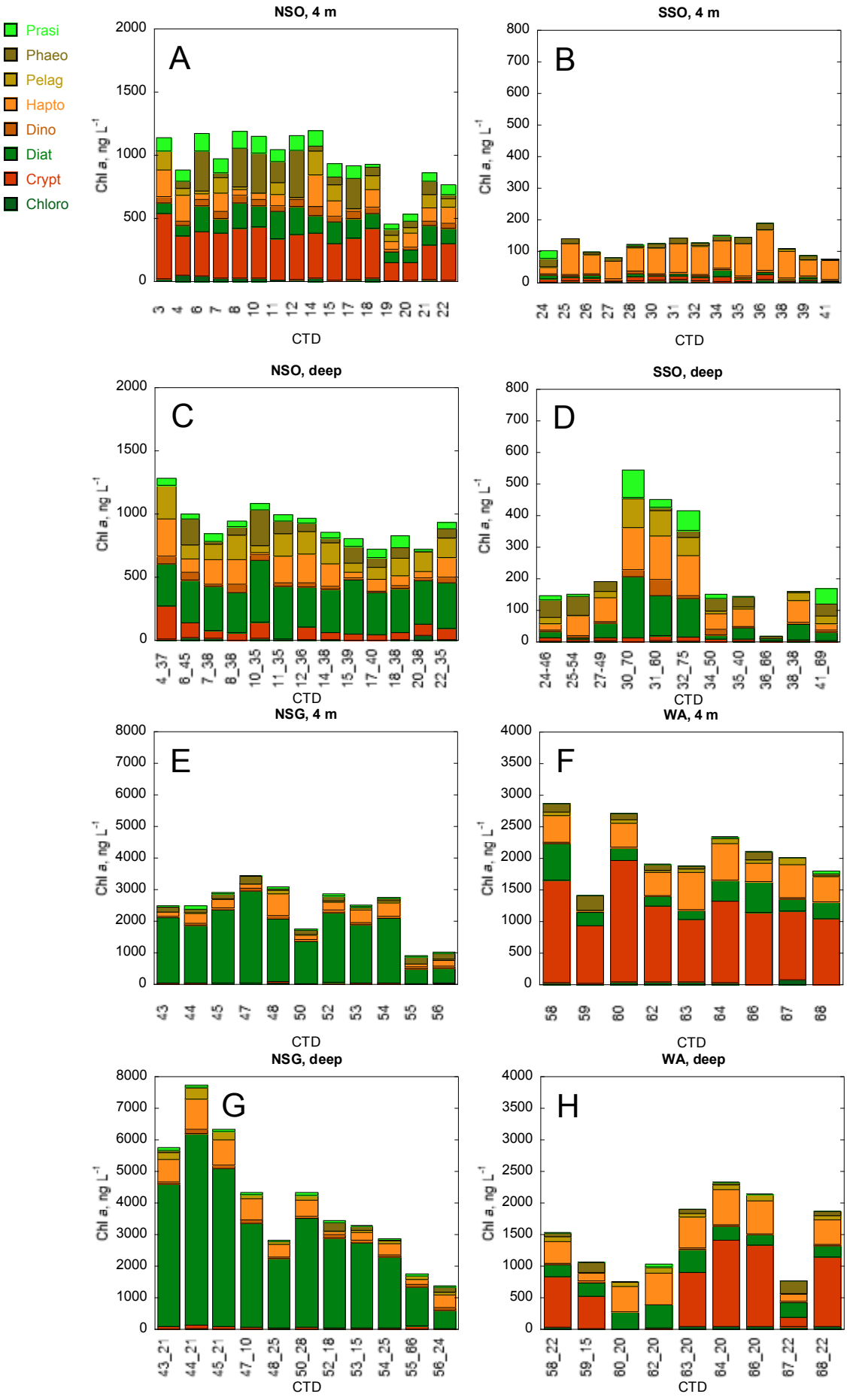
Prasi
Phaeo
Pelag
Hapto
Dino
Diat
Crypt
Chloro
NSO, 4 m
A
SSO, 4 m
B
NSO, deep
C
SSO, deep
D
NSG, 4 m
E
WA, 4 m
F
NSG, deep
G
WA, deep
H
Chl a, ng L-1
CTD

Figure 5

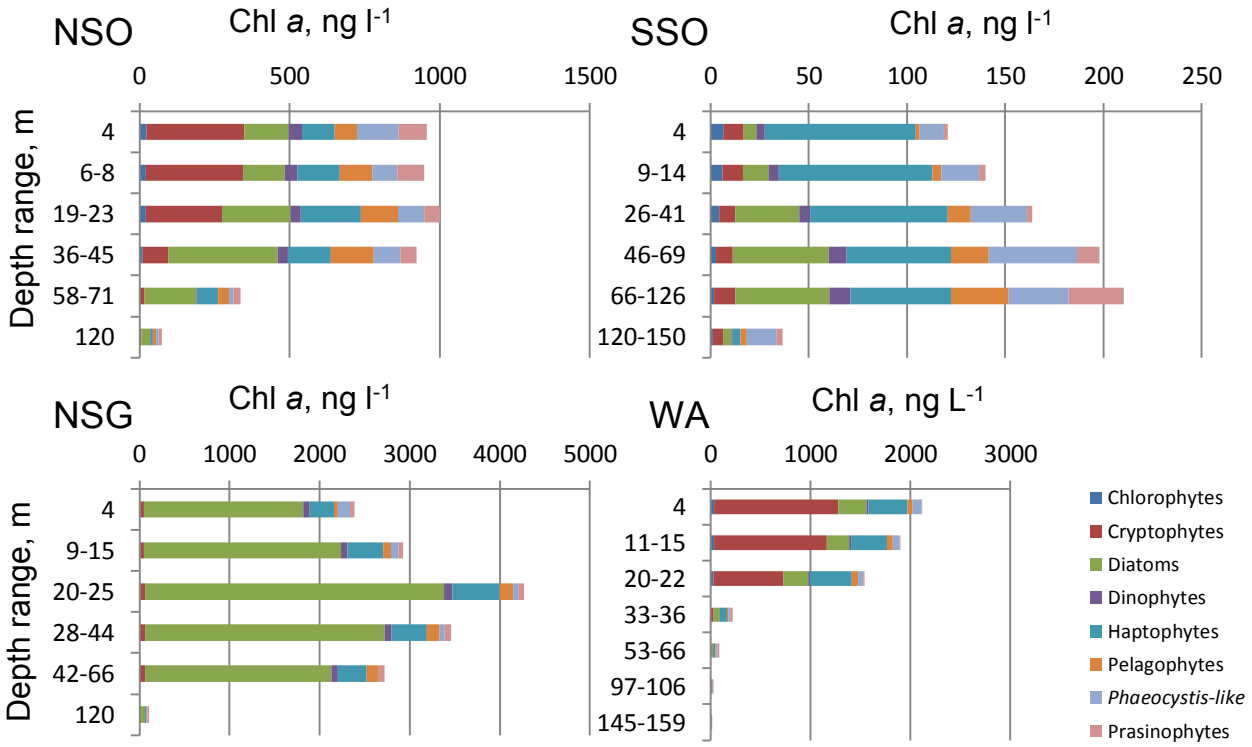
NSO
Chl a, ng l-1
0
500
1000
1500
Depth range, m
4
6-8
19-23
36-45
58-71
120
SSO
Chl a, ng l-1
0
50
100
150
200
250
4
9-14
26-41
46-69
66-126
120-150
NSG
Chl a, ng l-1
0
1000
2000
3000
4000
5000
Depth range, m
4
9-15
20-25
28-44
42-66
120
WA
Chl a, ng L-1
0
1000
2000
3000
4
11-15
20-22
33-36
53-66
97-106
145-159
Chlorophytes
Cryptophytes
Diatoms
Dinophytes
Haptophytes
Pelagophytes
Phaeocystis-like
Prasinophytes

Figure 6

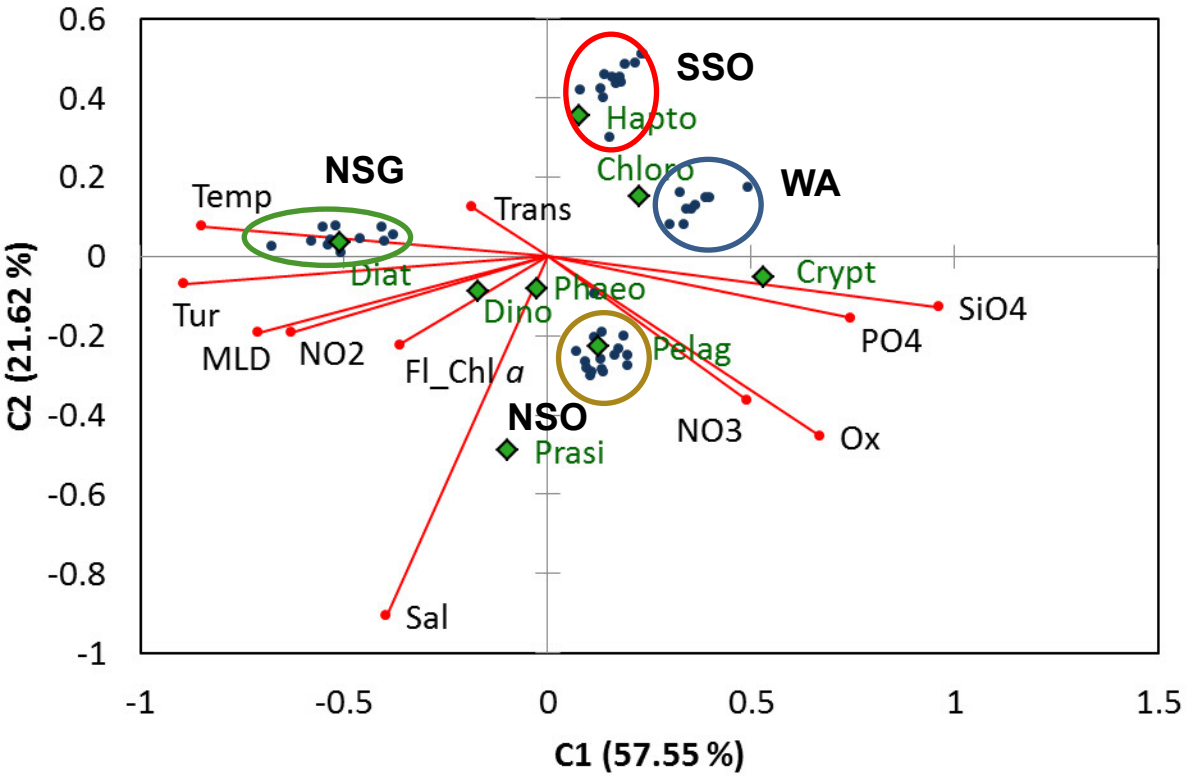
SSO
Hapto
NSG
Chloro
WA
Temp
Trans
Diat
Crypt
Phaeo
Tur
Dino
SiO4
PO4
MLD
NO2
Fl_Chl a
Pelag
NSO
NO3
Ox
Prasi
Sal
C2 (21.62 %)
C1 (57.55 %)
0.6
0.4
0.2
0
-0.2
-0.4
-0.6
-0.8
-1
-1
-0.5
0
0.5
1
1.5

Figure 7

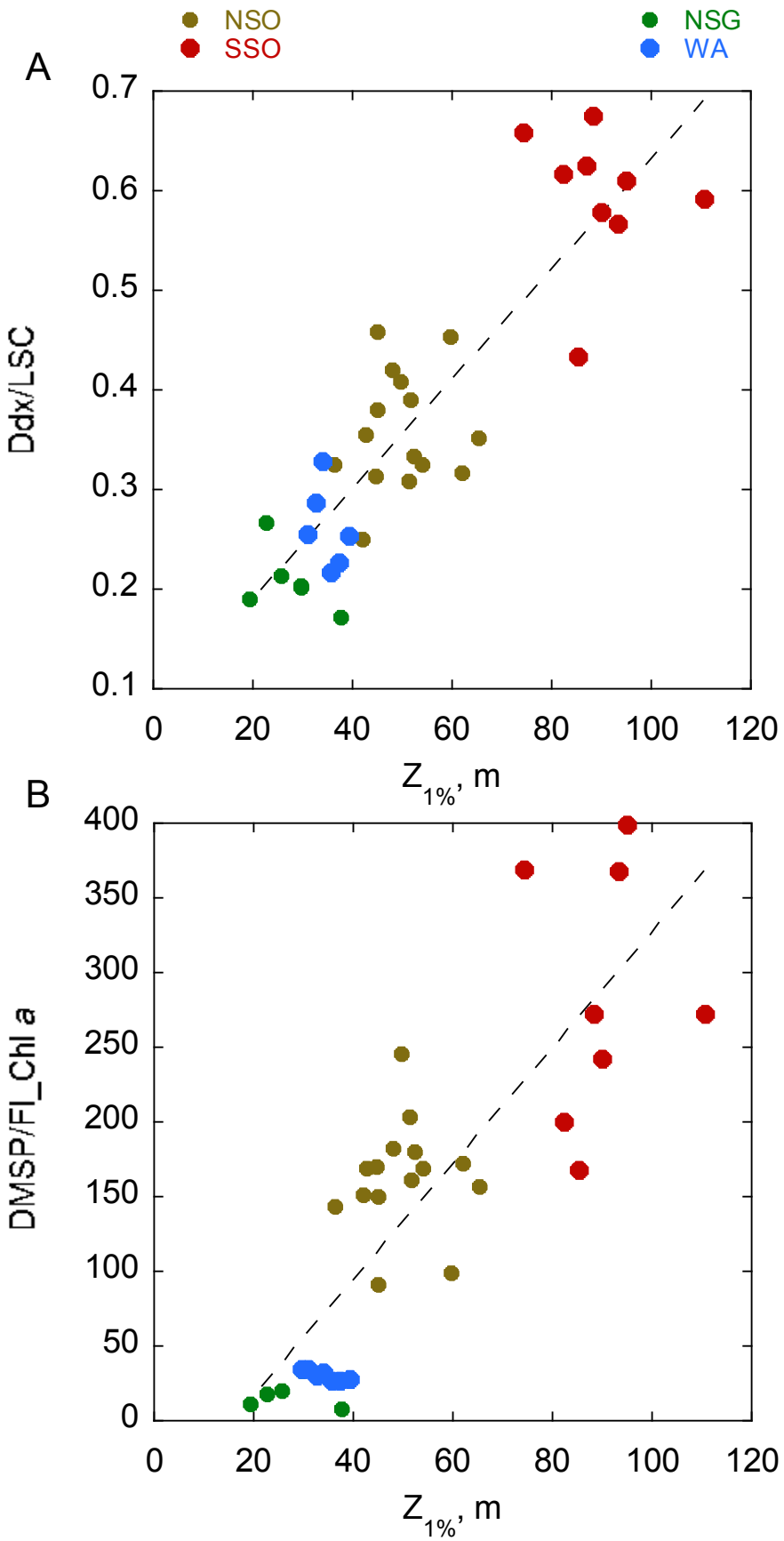
A
NSO
SSO
NSG
WA
Ddx/LSC
0.7
0.6
0.5
0.4
0.3
0.2
0.1
0
20
40
60
80
100
120
Z1%, m
B
DMSP/Fl_Chl a
400
350
300
250
200
150
100
50
0
0
20
40
60
80
100
120
Z1%, m

Figure 8

- Diatoms, cryptophytes and haptophytes were the most important chemotaxonomic groups
- Pelagophytes occurred in all study zones and were more abundant in subsurface waters
- Photoprotective pigment proportion was positively correlated with euphotic zone depth
- High DMSP/Chl*a* was associated with high irradiance and haptophyte relative abundance